41. Masuda,Y., Suzuki,M., Piao,J., Gu,Y., Tsurimoto,T. and Kamiya,K. (2007) Dynamics of human replication factors in the elongation phase of DNA replication. *Nucleic Acids Res.*, **35**, 6904–6916.
42. Tomida,J., Masuda,Y., Hiroaki,H., Ishikawa,T., Song,I., Tsurimoto,T., Tateishi,S., Shiomi,T., Kamei,Y., Kim,J. *et al.* (2008) DNA damage-induced ubiquitylation of RFC2 subunit of replication factor C complex. *J. Biol. Chem.*, **283**, 9071–9079.
43. Niwa,H., Yamamura,K. and Miyazaki,J. (1991) Efficient selection for high-expression transfectants with a novel eukaryotic vector. *Gene*, **108**, 193–199.
44. Maki,H. and Kornberg,A. (1987) Proofreading by DNA polymerase III of *Escherichia coli* depends on cooperative interaction of the polymerase and exonuclease subunits. *Proc. Natl Acad. Sci. USA*, **84**, 4389–4392.
45. Studier,F.W., Rosenberg,A.H., Dunn,J.J. and Dubendorff,J.W. (1990) Use of T7 RNA polymerase to direct expression of cloned genes. *Methods Enzymol.*, **185**, 60–89.
46. Siegel,L.M. and Monty,K.J. (1966) Determination of molecular weights and frictional ratios of proteins in impure systems by use of gel filtration and density gradient centrifugation. Application to crude preparations of sulfite and hydroxylamine reductases. *Biochim. Biophys. Acta*, **112**, 346–362.
47. Worthylake,D.K., Prakash,S., Prakash,L. and Hill,C.P. (1998) Crystal structure of the *Saccharomyces cerevisiae* ubiquitin-conjugating enzyme Rad6 at 2.6 Å resolution. *J. Biol. Chem.*, **273**, 6271–6276.
48. Yuasa,M.S., Masutani,C., Hirano,A., Cohn,M.A., Yamaizumi,M., Nakatani,Y. and Hanaoka,F. (2006) A human DNA polymerase η complex containing Rad18, Rad6 and Rev1; proteomic analysis and targeting of the complex to the chromatin-bound fraction of cells undergoing replication fork arrest. *Genes Cells*, **11**, 731–744.
49. Ahn,J.S. and Whitby,M.C. (2003) The role of the SAP motif in promoting Holliday junction binding and resolution by SpCCE1. *J. Biol. Chem.*, **278**, 29121–29129.
50. Chou,C.H., Wang,J., Knuth,M.W. and Reeves,W.H. (1992) Role of a major autoepitope in forming the DNA binding site of the p70 (Ku) antigen. *J. Exp. Med.*, **175**, 1677–1684.
51. Gohring,F., Schwab,B.L., Nicotera,P., Leist,M. and Fackelmayer,F.O. (1997) The novel SAR-binding domain of scaffold attachment factor A (SAF-A) is a target in apoptotic nuclear breakdown. *EMBO J.*, **16**, 7361–7371.
52. Kipp,M., Gohring,F., Ostendorp,T., van Drunen,C.M., van Driel,R., Przybylski,M. and Fackelmayer,F.O. (2000) SAF-Box, a conserved protein domain that specifically recognizes scaffold attachment region DNA. *Mol. Cell. Biol.*, **20**, 7480–7489.
53. Zhang,M., Windheim,M., Roe,S.M., Peggie,M., Cohen,P., Prodromou,C. and Pearl,L.H. (2005) Chaperoned ubiquitylation–crystal structures of the CHIP U box E3 ubiquitin ligase and a CHIP-Ubc13-Uev1a complex. *Mol. Cell*, **20**, 525–538.
54. Huang,A., Hibbert,R.G., de Jong,R.N., Das,D., Sixma,T.K. and Boelens,R. (2011) Symmetry and asymmetry of the RING-RING dimer of Rad18. *J. Mol. Biol.*, **410**, 424–435.
55. Gomes,X.V., Gary,S.L. and Burgers,P.M. (2000) Overproduction in Escherichia coli and characterization of yeast replication factor C lacking the ligase homology domain. *J. Biol. Chem.*, **275**, 14541–14549.

10394–10407 *Nucleic Acids Research, 2012, Vol. 40, No. 20* *Published online 16 August 2012*
doi:10.1093/nar/gks763

En bloc transfer of polyubiquitin chains to PCNA *in vitro* is mediated by two different human E2–E3 pairs

Yuji Masuda[1,2,*], Miki Suzuki[2], Hidehiko Kawai[3], Asami Hishiki[4], Hiroshi Hashimoto[4], Chikahide Masutani[1], Takashi Hishida[5], Fumio Suzuki[3] and Kenji Kamiya[2,*]

[1]Department of Genome Dynamics, Research Institute of Environmental Medicine, Nagoya University, Furo-cho, Chikusa-ku, Nagoya 464-8601, [2]Department of Experimental Oncology, [3]Department of Molecular Radiobiology, Research Institute for Radiation Biology and Medicine, Hiroshima University, 1-2-3 Kasumi, Minami-ku, Hiroshima 734-8553, [4]Graduate School of Nanobioscience, Yokohama City University, 1-7-29 Suehiro-cho, Tsurumi-ku, Yokohama 230-0045 and [5]Department of Molecular Genetics, Graduate School of Life Sciences, Gakushuin University, 1-5-1 Mejiro, Toshima-ku, Tokyo 171-8588, Japan

Received April 24, 2012; Revised July 5, 2012; Accepted July 18, 2012

ABSTRACT

Post-replication DNA repair in eukaryotes is regulated by ubiquitination of proliferating cell nuclear antigen (PCNA). Monoubiquitination catalyzed by RAD6–RAD18 (an E2–E3 complex) stimulates translesion DNA synthesis, whereas polyubiquitination, promoted by additional factors such as MMS2–UBC13 (a UEV–E2 complex) and HLTF (an E3 ligase), leads to template switching in humans. Here, using an *in vitro* ubiquitination reaction system reconstituted with purified human proteins, we demonstrated that PCNA is polyubiquitinated predominantly via *en bloc* transfer of a pre-formed ubiquitin (Ub) chain rather than by extension of the Ub chain on monoubiquitinated PCNA. Our results support a model in which HLTF forms a thiol-linked Ub chain on UBC13 (UBC13~Ub_n) and then transfers the chain to RAD6~Ub, forming RAD6~Ub_{n+1}. The resultant Ub chain is subsequently transferred to PCNA by RAD18. Thus, template switching may be promoted under certain circumstances in which both RAD18 and HLTF are coordinately recruited to sites of stalled replication.

INTRODUCTION

DNA is continuously injured by environmental insult as well as endogenous metabolic products. Such DNA damage, unless removed by multiple mechanisms for excision repair, inhibits replicative DNA polymerase action during DNA replication (1). Post-replication repair, to restart DNA replication stalled at DNA damaged sites, features two sub-pathways, translesion DNA synthesis (TLS) and template switching (TS), which are regulated by mono- and polyubiquitination of proliferating cell nuclear antigen (PCNA) at Lys164, respectively (2). RAD6 (an E2 ubiquitin-conjugating enzyme) and RAD18 (an E3 ubiquitin ligase) together catalyze the monoubiquitination of PCNA (2–4). The resultant monoubiquitinated PCNA (monoUb-PCNA) then activates the TLS pathway, in which stalled replication proceeds beyond the damage site with the help of specialized TLS polymerases. MonoUb-PCNA is believed to stimulate the entry of TLS polymerases at stalled 3′-ends, and this activity is dependent on interactions between the ubiquitin (Ub) moiety of monoUb-PCNA and the Ub-binding domains of the TLS polymerases (5–9). However, TLS is a mutagenic process due to the utilization of damaged templates by low-fidelity TLS polymerases (1).

Polyubiquitination of PCNA requires a different E2–E3 pair, MMS2–UBC13, a stable complex of an ubiquitin E2 variant (UEV) and an E2, and RAD5 in yeast (hereafter referred to as yRAD5) (2) or in humans, the two RAD5 homologs, HLTF and SHPRH, which serve as the E3 ligase (10–14). MMS2–UBC13 complexes mediate the formation of ubiquitin chains with Lys63 linkages (15). Polyubiquitinated PCNA (polyUb-PCNA) promotes the TS pathway, in which the primer end stalled at the

*To whom correspondence should be addressed. Tel: +81 52 789 3871; Fax: +81 52 789 3890; Email: masuda@riem.nagoya-u.ac.jp
Correspondence may also be addressed to Kenji Kamiya. Tel: +81 82 257 5842; Fax: +81 82 257 5844; Email: kkamiya@hiroshima-u.ac.jp

The authors wish it to be known that, in their opinion, the first two authors should be regarded as joint First Authors.

damaged site is released from the damaged template and anneals with the newly synthesized daughter strand of the sister chromosome. The molecular mechanism(s) of TS are currently unknown, but it is believed that a complex set of biochemical reactions is involved. When the sophisticated TS reactions are successfully performed, this process is essentially error-free, as it utilizes a non-damaged template (1).

It has been argued, mainly on the basis of genetic data from yeast studies, that polyubiquitination of PCNA is downstream of monoubiquitination. Both mono- and polyubiquitination are dependent on yRAD6 and yRAD18; deletion or mutation of either one of these two proteins blocks both the TS and TLS pathways. By contrast, inactivation or deletion of yMMS2, yUBC13 or yRAD5 abolishes polyubiquitination of PCNA, but not monoubiquitination of PCNA, and thus blocks only the TS pathway (1,2). These data are consistent with results previously obtained from *in vitro* biochemical studies using purified yeast enzymes (16,17). The yRAD6–yRAD18 complex can monoubiquitinate PCNA at Lys164, whereas yMMS2–yUBC13 and yRAD5 are able to polyubiquitinate PCNA only in the presence of yRAD6–yRAD18 (16). There is general agreement that the ligase activity of yRAD5 mediates sequential transfer of Ub from yUBC13~Ub to monoUb-PCNA (16,17). An unresolved issue, however, is why the error-free TS pathway would require the formation of monoUb-PCNA as an intermediate, which could potentially promote the error-prone TLS pathway and interfere with the preservation of genetic information.

In the current study, we investigated the mechanism of PCNA polyubiquitination using an *in vitro* ubiquitination reaction system reconstituted with purified recombinant human proteins, including HLTF. The results point to the existence of a novel reaction mechanism for the polyubiquitination of PCNA via *en bloc* Ub chain transfer. Importantly, the reaction mechanism appears to be more efficient than the conventional mechanism of sequential addition of Ub monomers to the distal end of an Ub chain on PCNA. We discuss the implications of these *in vitro* findings in terms of the choice of pathway, TS or TLS, proceeding from stalled replication sites following DNA damage.

MATERIALS AND METHODS

Plasmids

Expression plasmids for PCNA, RFC, E1, RAD6A, the RAD6A–RAD18 complex and Ub have been described previously (7,18–21). Expression plasmids for MMS2 and UBC13 were constructed using the pET20 parental vector. For the production of MMS2–UBC13 complexes, *MMS2* and *UBC13* were co-expressed as a single operon under the control of the T7 promoter. *HLTF* was cloned into pBAD22A (obtained from National BioResource Project, National Institute of Genetics, Mishima, Japan), and expression was induced by arabinose. For the histidine-tagged proteins, the tag sequence of pET15 was ligated to the 5′-end of the start codons of the respective genes. For $^{His}USP2^{(258-605)}$, a truncated sequence corresponding to amino acids 258–605 was subcloned into pET15. Synthetic genes encoding the $^{His}PCNA–Ub^{GG}$ fusion proteins were constructed in pET28a.

Proteins

Isopeptidase T was purchased from Boston Biochem (E-322). Other recombinant human proteins were expressed in *Escherichia coli* strain BL21 (DE3) at 15°C and then purified by chromatography at 4°C using the indicated columns (GE Healthcare), unless otherwise indicated. PCNA, RFC, E1, RAD6A, RAD6A–RAD18 complexes and Ub were purified as described previously (7,18,19,21). MMS2–UBC13 complexes were purified by sequential chromatography on HiPrep DEAE FF, HiTrap SP XL, HiTrap SP HP, HiTrap Heparin HP and Superdex 200 columns. MMS2–$UBC13^{C87A}$ complexes were purified on HiTrap Heparin HP, HiTrap SP XL and HiTrap SP HP columns, and MMS2–^{FLAG}UBC13 complexes were purified on HiTrap Q FF, HiTrap SP HP and HiTrap Heparin HP columns. UBC13 was purified on HiPrep DEAE FF, HiTrap SP FF, HiTrap SP HP, HiTrap Heparin HP and Superdex 200 columns. HLTF was purified on HiTrap Heparin HP, HiTrap SP HP, HiTrap Q HP, HiTrap SP XL, Econopack CHT-II (BIO-RAD) and Superdex 200 columns. RAD6A–^{His}RAD18, ^{His}HLTF and the corresponding mutants of each were partially purified using HiTrap Chelating HP and Superdex 200 columns. ^{His}PCNA, $^{His}PCNA–Ub^{K63R/\Delta GG}$ and $^{His}PCNA^{K164R}–Ub^{\Delta GG}$ were purified using HiTrap Chelating HP, HiTrap Q FF and Superdex 200 columns. $^{His}USP2^{(258-605)}$ was purified using HiTrap Chelating HP and Superdex 200 columns. MonoUb-PCNA was purified from *E. coli* overexpressing PCNA, E1 and RAD6A–RAD18, and ^{His}Ub. ^{His}yRAD5 was overexpressed in strain BL21 Star (DE3) (Life Technologies), which harbors pMStRNA1 (22), and partially purified using a HiTrap Chelating HP column.

Ubiquitination assays

The standard reaction mixture (25 µl) contained 20 mM HEPES–NaOH (pH 7.5), 50 mM NaCl, 0.2 mg/ml BSA, 1 mM DTT, 10 mM $MgCl_2$, 1 mM ATP, poly(dA)-oligo(dT) (GE Healthcare) (100 ng) as the source of multiple primed single-stranded (mpss) DNA, PCNA (1.0 pmol trimer), RFC (0.70 pmol), E1 (0.85 pmol), RAD6A–RAD18 complexes (0.54 pmol trimer), MMS2–UBC13 complexes (16.4 pmol dimer), HLTF (1.3 pmol) and Ub (174 pmol). For the competition assays containing 1740 pmol Ub, 6 pmol E1 was introduced to overcome the inhibitory effect of large amounts of Ub (23,24). Reaction mixtures were prepared on ice and then incubated at 30°C for 10 min unless otherwise indicated. Reaction products were analyzed by immunoblot. Where indicated by 'reducing' or unless otherwise indicated, the samples were treated with sodium dodecyl sulphate (SDS) sample buffer containing 280 mM β-mercaptoethanol. Samples that were not treated with reducing agent were referred to as 'non-reducing'. Anti-PCNA (Santa Cruz, sc-7907), anti-UBC13 (IMGENEX, IMG-5634), anti-RAD6

(Abcam, ab31917), anti-Ub (Sigma, U5379) and anti-FLAG M2 monoclonal antibodies (Sigma, F 3165) were used as indicated. Immunoreactive proteins were visualized using an ECL chemiluminescence kit (GE Healthcare).

Ub transfer assays of UBC13~Ub

The reaction mixture (25 µl) contained 20 mM HEPES–NaOH (pH 7.5), 50 mM NaCl, 0.2 mg/ml BSA, 1 mM DTT, 5 mM $MgCl_2$, 1 mM ATP, poly(dA)-oligo(dT) (GE Healthcare) (100 ng) as the source of mpssDNA, E1 (1.7 pmol), MMS2–UBC13 complexes (83.7 pmol dimer) and Ub (174 pmol). After incubation at 30°C for 10 min, the reactions were quenched by the addition of *N*-ethylmaleimide (NEM) (5 mM) and EDTA (25 mM) for 1 min (25,26). HLTF (1.3 pmol) was introduced and the mixture was allowed to incubate for an additional 2 min. Reaction products were analyzed by immunoblot.

Purification of ^{His}Ub-charged RAD6A–RAD18

The reaction mixture (5 ml) contained 20 mM HEPES–NaOH (pH 7.5), 5 mM $MgCl_2$, 1 mM ATP, E1 (1.2 nmol), RAD6A–^{His}RAD18 complexes (partially purified fraction, ~3 nmol trimer) and ^{His}Ub (46 nmol). After incubation at 20°C for 10 min, the mixture was immediately applied to a HiTrap Heparin HP column (1 ml) at 4°C. RAD6A–^{His}RAD18 complexes were eluted with a linear gradient of NaCl. Aliquots of peak fractions were frozen in liquid nitrogen and stored at −80°C.

RESULTS

Polyubiquitination of PCNA by *en bloc* Ub chain transfer

To explore the molecular mechanism of PCNA ubiquitination in humans, we developed an *in vitro* ubiquitination reaction system reconstituted with recombinant human proteins (Supplementary Figure S1A) (7,19). As shown in Figure 1A, polyubiquitination of PCNA was readily apparent when MMS2–UBC13 and HLTF-containing reactions were supplemented with RAD6A–RAD18, E1, mpssDNA and replication factor C (RFC), a PCNA loader, all of which are required for PCNA monoubiquitination (7,13). No PCNA ubiquitination was detected when RAD6A–RAD18 or E1 was omitted, or when PCNA was replaced with a mutant derivative carrying a K164R single amino acid substitution; small amounts of ubiquitinated PCNA were observed when mpssDNA or RFC was omitted. When Ub was replaced with an Ub^{K63R} mutant, only monoUb-PCNA was observed, which suggested that the Ub chain linkage was via a Lys63 linkage (Figure 1B) (13).

Analysis of the time course of the reaction indicated that the accumulation of polyubiquitinated products was consistent over time, as opposed to smaller products forming first and then gradually converting into larger products (Figure 1C). This property was consistently observed under other assay conditions with different enzyme concentrations (Supplementary Figure S2). These results suggested that PCNA polyubiquitination may take place via *en bloc* transfer of a Ub chain (27) that is first formed on E2 via a thioester bond at a catalytic cysteine (E2~Ub_n) (Figure 1D), and then transferred to PCNA. To test this hypothesis, the presence of unanchored Ub chains was assessed by immunoblot following treatment with a reducing agent, to hydrolyze the thioester bond of E2~Ub_n (25). Following SDS–polyacrylamide gel electrophoresis (PAGE), immunoblot analysis with an anti-Ub antibody showed the formation of unanchored Ub chains with Lys63 linkages (Figure 1E and F). Efficient formation of Ub multimers was completely dependent on MMS2–UBC13 and E1, but not on RAD6–RAD18, RFC or PCNA. Interestingly, Ub multimer formation required the presence of HLTF and mpssDNA, while a small amount of Ub_2 was formed in their absence, as previously observed when Ub was incubated with MMS2–UBC13 and E1 (15,28). To obtain direct evidence of UBC13~Ub_n formation, reactions were analyzed by SDS–PAGE under non-reducing conditions in order to prevent hydrolysis of the thioester bond, followed by immunoblot analysis with an anti-UBC13 antibody (25). The results clearly demonstrated the formation of UBC13~Ub_n (Figure 1G), which disappeared upon treatment with a reducing agent (Figure 1H). There was only slight accumulation of UBC13 conjugated to long chain Ub (>Ub_5) (Figure 1G), which was in contrast to polyubiquitinated PCNA and unanchored Ub chains, where larger products were relatively abundant (Figure 1A and E; see also 'Discussion' section). The protein components required for efficient UBC13~Ub_n ($n \geq 2$) formation (Figure 1G) were the same as those required for unanchored Ub multimer formation (Figure 1E). Notably, when either HLTF or mpssDNA was omitted, formation of Ub chains and UBC13~Ub_n was severely reduced. Small amounts of Ub_2 and UBC13~Ub_2 were detected, however, and this was dependent on MMS2–UBC13 (Figure 1E and G). These results suggested that mpssDNA is involved in the same biochemical step as HLTF, probably as a co-factor in Ub chain formation.

To test this putative mechanism of *en bloc* Ub chain transfer of preformed chains of UBC13~Ub_n to PCNA, we examined whether pre-incubation of MMS2–UBC13 and HLTF with Ub before the addition of PCNA could accelerate the immediate formation of poly-Ub PCNA with long Ub chains. We set up the following experiments, as shown in Figure 1I. In Ex. 1, RAD6A–RAD18, MMS2–UBC13, E1, Ub, mpssDNA and HLTF were pre-incubated for 5 min, and then combined with a PCNA–preassembly mixture containing PCNA, RFC and mpssDNA. In Ex. 2, RAD6A–RAD18, MMS2–UBC13, E1, Ub and mpssDNA were pre-incubated for 5 min and then combined with a PCNA–preassembly mixture together with HLTF. After a brief period of additional incubation for 15 s, the reaction products were analyzed by immunoblot using an anti-PCNA antibody. In Ex. 1, but not Ex. 2, Ub chains would be assembled on E2 by HTLF prior to the addition of PCNA for *en bloc* Ub chain transfer; by contrast, a step-wise addition of Ub onto PCNA would yield similar kinetics in both experiments. A different size distribution of poly-Ub PCNA was

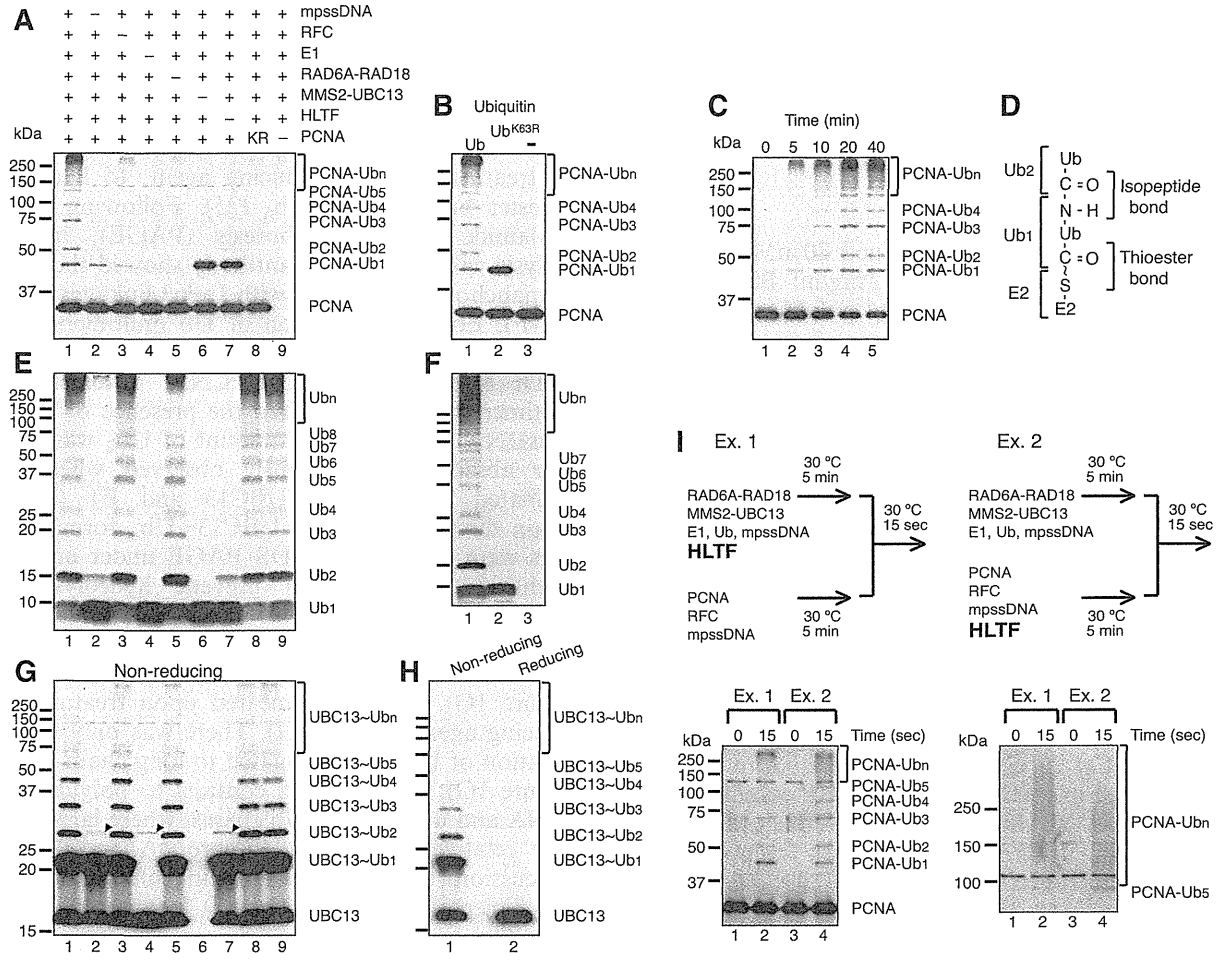

Figure 1. Polyubiquitination of PCNA by *en bloc* Ub chain transfer. (**A**) *In vitro* reconstituted PCNA polyubiquitination reactions. Reactions were reconstituted with PCNA, mpssDNA, RFC, E1, RAD6A–RAD18, MMS2–UBC13, HLTF and Ub. Reaction products were analyzed by immunoblot using an anti-PCNA antibody. –, omitted factor; KR, $PCNA^{K164R}$. (**B**) Lys63-linked Ub chain formation on PCNA was analyzed by immunoblot using an anti-PCNA antibody. (**C**) Time course of polyubiquitination. Reaction products were analyzed by immunoblot using an anti-PCNA antibody. (**D**) Chemical structure of the thiol-linked Ub dimer on E2 ($E2{\sim}Ub_2$). (**E** and **F**) Unanchored Ub chain formation. The products of (A) and (B) were probed with an anti-Ub antibody in (E) and (F), respectively. In these blots, the signals corresponding to ubiquitinated PCNA are not detectable. The amount of PCNA trimer in the reaction was 1 pmol (3 pmol monomer), whereas the amount of ubiquitin was 174 pmol; thus, the estimated signal intensity of total ubiquitinated PCNA was <1% that of ubiquitin. (**G** and **H**) $UBC13{\sim}Ub_n$ formation. The products of (A) untreated by a reducing agent were probed with an anti-UBC13 antibody (G). Presumed dimers of UBC13 linked via S–S bond formation during sample preparation are indicated by arrowheads. The products of lane 1 in (G) treated with or without a reducing agent were analyzed by immunoblot using an anti-UBC13 antibody (H). (**I**) Transfer of pre-formed Ub chains to PCNA. The experimental designs are shown in the upper panel (see text for details). The reaction products were analyzed by electrophoresis under two different conditions and then probed with an anti-PCNA antibody.

observed under the two reaction conditions (Figure 1I and Supplementary Figure S3). In Ex. 1, the accumulation of large products (>150 kDa) was quite prominent. In contrast, in Ex. 2, intermediate sized poly-Ub PCNA (50 to ≤ 150 kDa) was abundant, but large products (>250 kDa) were much less abundant compared to Ex. 1. These results supported *en bloc* Ub chain transfer under these *in vitro* experimental conditions. To obtain further evidence, we analyzed detailed mechanisms underlying the hypothesized *en bloc* Ub chain transfer in additional experiments (see below).

Essential function of HLTF in $UBC13{\sim}Ub_n$ formation

To further investigate the role of HLTF in PCNA polyubiquitination, we analyzed $UBC13{\sim}Ub_n$ formation separately from PCNA polyubiquitination. The minimal set of factors necessary for $UBC13{\sim}Ub_n$ formation (Figure 2A) as well as for unanchored Ub chain formation (Figure 2B) were HLTF, MMS2–UBC13, E1, Ub and mpssDNA. Replacing wild-type Ub with its mutant derivative, Ub^{K63R}, confirmed that the multiple bands observed were Lys63-linked Ub chains on UBC13 (Figure 2C, lane 4). Furthermore, when Ub was replaced with ^{FLAG}Ub, the bands migrated more slowly (Figure 2C, lane 3), which indicated that they contained Ub molecules.

The RING domain of E3 serves an essential function in the ligase reaction by mediating the interaction with E2 (29,30). To determine whether the ligase activity of HLTF was necessary for Ub chain formation, we constructed an HLTF RING mutant in which the conserved cysteine

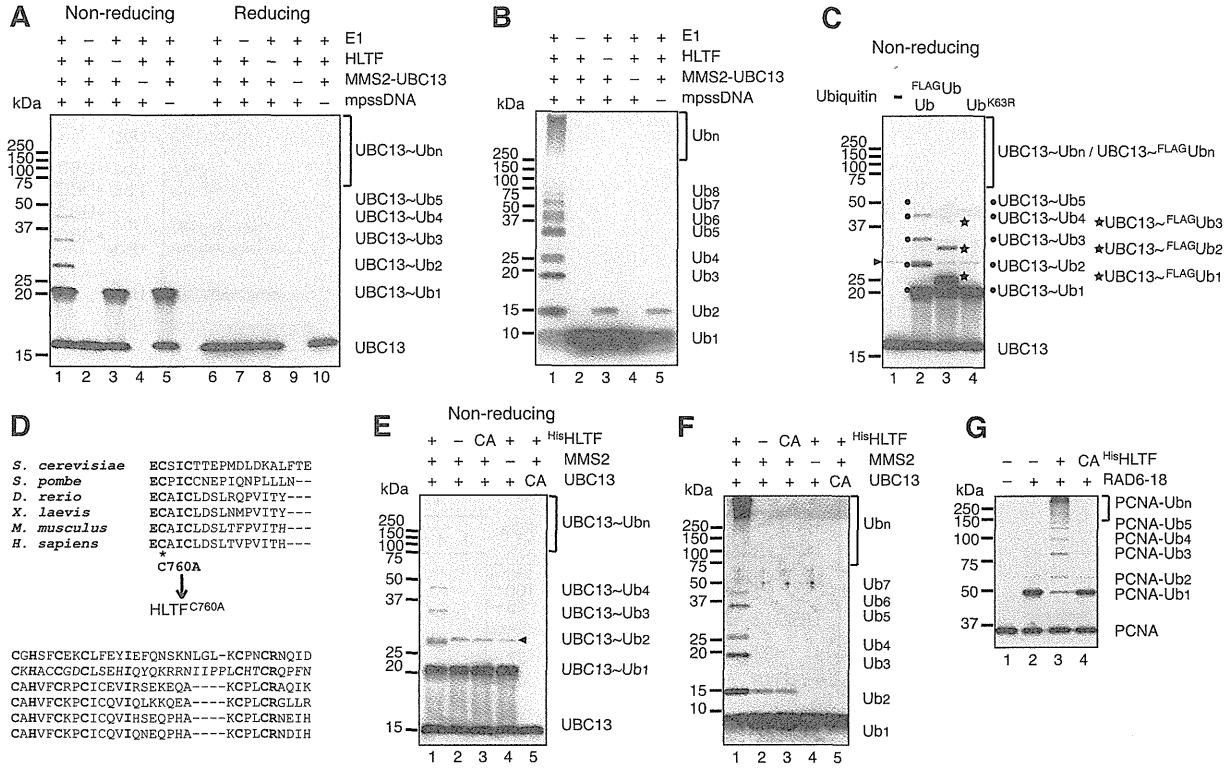

Figure 2. Analysis of UBC13~Ub_n formation. (**A**) Formation of thiol-linked Ub chains on UBC13 with the minimal set of factors. The reactions were reconstituted with mpssDNA, E1, MMS2–UBC13, HLTF and Ub. The reaction products treated with or without a reducing agent were analyzed by immunoblot using an anti-UBC13 antibody. –, omitted factor. (**B**) Formation of Ub chains with the minimal set of factors. The reaction products in (A) were treated with a reducing agent and then analyzed by immunoblot using an anti-Ub antibody. (**C**) Evidence that the multiple thiol-linked bands on UBC13 are Lys63-linked Ub chains. The reaction products untreated by a reducing agent were analyzed by immunoblot using an anti-UBC13 antibody. The positions of UBC13~Ub_n and UBC13~$^{FLAG}Ub_n$ are indicated by dots and stars, respectively. Presumed dimers of UBC13 linked via S–S bond formation during sample preparation are indicated by an arrowhead. (**D**) Multiple sequence alignment of the RING fingers of human HLTF and its orthologs. The conserved cysteine residue (marked with asterisk) was replaced with an alanine. (**E** and **F**) Analysis of HLTF mutants. The reaction products were treated with (F) or without (E) a reducing agent and then analyzed by immunoblot using an anti-UBC13 antibody (E) and an anti-Ub antibody (F). –, omitted factor; CA for ^{His}HLTF, ^{His}HLTF^{C760A}; CA for UBC13, UBC13^{C87A}. Presumed dimers of UBC13 linked via S–S bond formation during sample preparation are indicated by an arrowhead. (**G**) Catalytic activity of HLTF is essential for polyubiquitination of PCNA. PCNA polyubiquitination reactions were performed using ^{His}HLTF or ^{His}HLTF^{C760A} (CA) under standard reaction conditions. The reaction products were analyzed by immunoblot using an anti-PCNA antibody.

residue (C760) of the RING domain was replaced with an alanine (Figure 2D). Histidine-tagged wild-type and mutant HLTF (^{His}HLTF and ^{His}HLTF^{C760A}, respectively) were partially purified (Supplementary Figure S1B) and eluted in the same fraction as untagged HLTF from a gel filtration column, which confirmed the integrity of them to be preserved. ^{His}HLTF was able to support Ub chain formation as efficiently as untagged HLTF, whereas the mutant protein was unable to do so (Figure 2E and F, lanes 3). Thus, Ub chain formation was dependent on the E3 ligase activity of HLTF. Additionally, a mutant form of UBC13 (UBC13^{C87A}) (Supplementary Figure S1B), in which the conserved cysteine residue involved in thioester bond formation with Ub was replaced with alanine, did not support chain formation (Figure 2E and F, lanes 5). Finally, replacing MMS2–UBC13 complexes with UBC13 monomers (Supplementary Figure S1B) demonstrated that MMS2 was also required for Ub chain formation (Figure 2E and F, lanes 4).

Using the HLTF RING mutant, we confirmed that the catalytic activity of HLTF was required for PCNA polyubiquitination, as well as for UBC13~Ub_n formation (Figure 2G). These results were consistent with the idea that HLTF mediates UBC13~Ub_n formation and then the resultant Ub chain is transferred *en bloc* to PCNA.

Analysis of UBC13~Ub_n formation

UBC13-linked polyubiquitin chains could be generated through an aminolysis-based transfer reaction between neighboring UBC13~Ub molecules, in which the ε-amino group of Lys63 of one Ub molecule attacks the thioester-linked carbonyl of the neighboring Ub molecule on UBC13 (25,27) (Figure 3A, schematic). To investigate this as a possible mechanism, UBC13 in complex with MMS2 was first charged with either wild-type Ub or Ub^{K63R} in the presence of E1 and mpssDNA for 10 min. After quenching for 1 min, by the addition of NEM and EDTA, to inactivate uncharged UBC13 and E1 (25,26), the reaction mixture was supplemented with HLTF and then incubated for an additional 2 min. HLTF-dependent Ub chain formation, as evidenced by the appearance of UBC13~Ub_n ($n \geq 3$), was observed with Ub, but not with Ub^{K63R} (Figure 3B), although a significant amount of

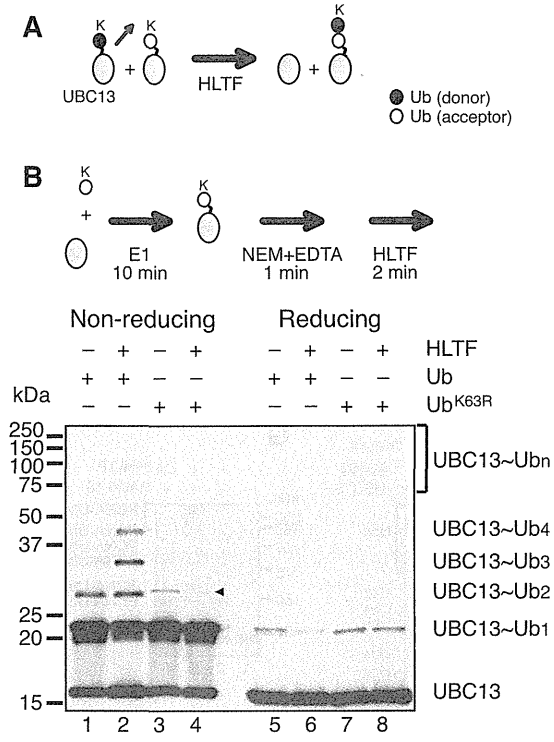

Figure 3. Ub transfer reactions between UBC13~Ub molecules. (**A**) A proposed mechanism of E2~Ub_n formation. A red arrow depicts the direction of Ub movement. MMS2 was included in the reactions by omitted from the schematic. (**B**) Analysis of Ub transfer reactions between UBC13~Ub molecules. The experimental design is shown in the upper panel (see text for details). The reactions were reconstituted with the minimal set of factors (mpssDNA, E1, MMS2–UBC13, HLTF and Ub). The reaction products were treated with or without a reducing agent and then analyzed by immunoblot using an anti-UBC13 antibody. –, omitted factor. Presumed dimers of UBC13 linked via S–S bond formation during sample preparation are indicated by an arrowhead.

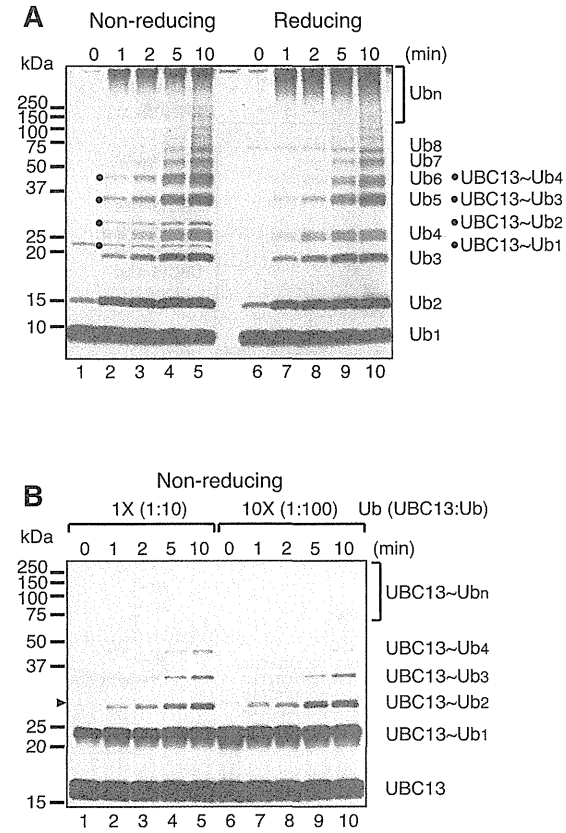

Figure 4. Preferential utilization of UBC13~Ub as Ub acceptor by HLTF. (**A**) Time-course of chain formation using the minimal set of factors. Reaction mixtures containing mpssDNA, E1, MMS2–UBC13 and Ub were pre-incubated for 10 min and then the reactions were started by adding HLTF and incubated for the indicated times. Reaction products were treated with or without a reducing agent and then analyzed by immunoblot using an anti-Ub antibody. (**B**) UBC13~Ub_n competition assays. Reactions in the presence of a 10-fold excess of Ub (10×) were compared to those under standard reaction conditions (1×) with the minimal set of factors. The molecular ratios of UBC13 to Ub are shown in parentheses. Reaction mixtures were pre-incubated without HLTF for 1 min and then the reactions were started by adding HLTF and incubated for the indicated times. Reaction products untreated by a reducing agent were analyzed by immunoblot using an anti-UBC13 antibody. Presumed dimers of UBC13 linked via S–S bond formation during sample preparation are indicated by an arrowhead.

UBC13~Ub_2 was formed in the absence of HLTF under these reaction conditions (Figure 3B, lane 1). The reaction products were sensitive to treatment with a reducing agent, which indicated that they possessed thiol-linked Ub chains (Figure 3B, lanes 5–7). We also confirmed that UBC13~Ub_n formed in these reactions was not a product of recharging due to incomplete quenching (Supplementary Figure S4; see also Supplementary Note for Supplementary Figure S4). Collectively, these results demonstrated that HLTF catalyzes UBC13-Ub_n formation by enhancing an aminolysis-based transfer reaction between two UBC13~Ub molecules.

Preferential utilization of UBC13~Ub as a Ub acceptor by HLTF

Next, we investigated whether the transfer reaction between two UBC13~Ub molecules, as depicted in Figure 3A, was the predominant mechanism, or if Ub moieties from UBC13~Ub were transferred to uncharged Ub as well as a UBC13~Ub. This was addressed by analyzing the time course of the reaction. Reaction mixtures were pre-incubated without HLTF for 10 min, and then reaction products were removed at different time points after the addition of HLTF and analyzed by immunoblot using an anti-Ub antibody (Figure 4A). Comparison of the products formed under non-reducing and reducing conditions demonstrated that UBC13~Ub_n was present only under non-reducing conditions, while unanchored Ub chains were present under both conditions (Figure 4A; quantified in Supplementary Figure S5A). In all of these reactions, Ub was present in ~20-fold molecular excess over UBC13~Ub (see legend for Supplementary Figure S5B). Thus, if Ub was transferred to uncharged Ub as well as UBC13~Ub, the formation of unanchored Ub chains would predominate. However, unanchored and UBC13-linked Ub chains were detected at equivalent levels at the early time points (Figure 4A and Supplementary Figure S5A), which suggested that HLTF preferentially transfers Ub to UBC13~Ub rather than uncharged Ub, and that UBC13~Ub is a preferred Ub acceptor for HLTF (Supplementary Figure S5B).

To confirm the preferential utilization of UBC13~Ub as an Ub acceptor, the experiment was repeated, this time with Ub at 100-fold molar excess over UBC13 (Figure 4B). Under these conditions, excess Ub would strongly compete against UBC13~Ub_n formation. Alternatively, if UBC13~Ub was the preferred substrate, UBC13~Ub_n formation would be unaffected by excess Ub. The time course of the reaction clearly showed only a slight inhibitory effect of 100-fold excess Ub (<2-fold), providing additional evidence of the specificity of HLTF for UBC13~Ub as a Ub acceptor. Additionally, we demonstrated that the formation of unanchored Ub chains was strongly decreased at low concentrations of uncharged Ub (Supplementary Figure S6 and Supplementary Note for Supplementary Figure S6), which indicated that the unanchored Ub chains were by-products generated, at least in part, by Ub (chain) transfer from UBC13~Ub_n ($n \geq 1$) to uncharged Ub (see Supplementary Note for Supplementary Figure S6).

Analysis of the mechanism of polyubiquitination of PCNA

One current theory of polyubiquitination of PCNA holds that the Ub chain forms on the Ub moiety of monoUb-PCNA, and that the role of RAD6A–RAD18 is simply to provide a source of monoUb-PCNA. Based on this model, RAD6A–RAD18 should be dispensable when pre-formed monoUb-PCNA is supplied as the substrate for the polyubiquitination reaction, as was previously shown using yeast proteins (16). To examine the Ub transfer reaction in more detail, partially ^{His}Ub-modified PCNA (PCNA-^{His}Ub) was purified and used as the substrate. In contrast to previous reports using yRAD5, monoUb-PCNA was a surprisingly poor substrate for PCNA polyubiquitination upon incubation with E1, MMS2–UBC13 and HLTF, although trace amounts of polyUb-PCNA were detected (Figure 5A, lane 2 and Figure 5B, lanes 1–5). When RAD6A–RAD18 was added to the reaction mixture, however, polyUb-PCNA was efficiently generated (Figure 5A, lane 5 and Figure 5B, lanes 6–10). It appeared that polyUb-PCNA species were derived from unmodified PCNA rather than from PCNA-^{His}Ub, because the amount of unmodified PCNA was significantly reduced upon prolonged incubation, while that of PCNA-^{His}Ub remained unchanged (Figure 5B, lanes 6–10). The poor capacity of PCNA-^{His}Ub to act as a substrate for polyubiquitination was not due to any intrinsic property of ^{His}Ub, because it was an excellent substrate for polyubiquitination of unmodified PCNA (Supplementary Figure S7). Furthermore, we also tested a PCNA–Ub^{GG} fusion protein, in which Ub was fused to the C-terminus of PCNA via a six amino acid linker, and the two glycine residues in the C-terminus of the Ub moiety were deleted to avoid aberrant charging reactions (Figure 5C). Here, two different ^{His}PCNA–$Ub^{\Delta GG}$ fusion proteins carrying either a K164R mutation in PCNA or a K63R mutation in Ub were examined. Polyubiquitination of ^{His}PCNA–$Ub^{K63R/\Delta GG}$ was much more prominent than with ^{His}PCNA^{K164R}–Ub^{GG} (Figure 4C), which suggested that HLTF does not prefer the Ub moiety of the ^{His}PCNA–Ub^{GG} fusion protein as an acceptor.

The results described above suggested a novel mechanism of polyubiquitination of PCNA, in which mono- and polyubiquitination are coupled to a certain extent. One possibility is that Ub chains are formed directly on Lys164 of PCNA by HLTF and that RAD6–RAD18 is required for a non-catalytic function. To test this hypothesis, we used a RING mutant of RAD18, in which the conserved isoleucine (I50) and arginine (R51) residues were replaced with alanine (Figure 5D); this mutant has been shown to have reduced ligase activity (21). Histidine-tagged wild-type RAD18 and mutant RAD18 (^{His}RAD18 and ^{His}RAD18$^{I50A/R51A}$, respectively) were partially purified in complex with RAD6A (Supplementary Figure S1D). The protein complexes eluted in the same fraction as untagged RAD6A–RAD18 in gel filtration chromatography, which confirmed the integrity of them to be preserved. RAD6A–^{His}RAD18 (wild-type) was able to support mono- and polyubiquitination of PCNA as well as untagged RAD6A–RAD18 (Figure 5E, lanes 1 and 5). By contrast, in the presence of the RAD18 mutant, very little monoUb- or polyUb-PCNA was produced in the presence or absence of HLTF (Figure 5E, lanes 2 and 6). We also examined a mutant form of RAD6A, RAD6A^{C88A}, in which a conserved cysteine residue (C88) involved in the formation of thioester bonds with Ub was replaced with an alanine. Similar to the RAD18 RING mutant, RAD6A^{C88A} did not support chain formation (Figure 5E, lanes 3 and 7). These results indicated that PCNA polyubiquitination depends on the catalytic cysteine of RAD6A and an intact RING finger of RAD18.

We next considered the possibility that Ub chains may first be formed via Lys63 of the thiol-linked Ub moiety on RAD6 by HLTF and then transferred, together with the proximal Ub pre-bound to RAD6, to Lys164 of PCNA by RAD18. In this case, thiol-linked Ub chains on RAD6A might be detected in a manner that is dependent on MMS2–UBC13 and HLTF. The products of the PCNA polyubiquitination reaction shown in Figure 1G were re-analyzed by immunoblot using an anti-RAD6 antibody. The results clearly demonstrated the formation of multiple RAD6A bands that were dependent on MMS2–UBC13, HLTF, mpssDNA and E1, but independent of PCNA and RFC (Figure 5F). These bands were also sensitive to treatment with a reducing agent (Figure 5G). Notably, RAD6A~Ub_n accumulated under conditions in which Ub chain transfer to PCNA was blocked, i.e. when RFC or PCNA was omitted (Figure 5F, lanes 3 and 9), when PCNA was replaced with PCNA^{K164R} (lane 8), or when the RING mutant of RAD18 was used (Figure 5H). These results strongly suggested that RAD6-linked Ub chains are intermediates between UBC13~Ub_n and polyUb-PCNA.

Analysis of RAD6A~Ub_n formation

Because the presence of RAD6A~Ub_n is a novel observation that has not been reported previously, we investigated

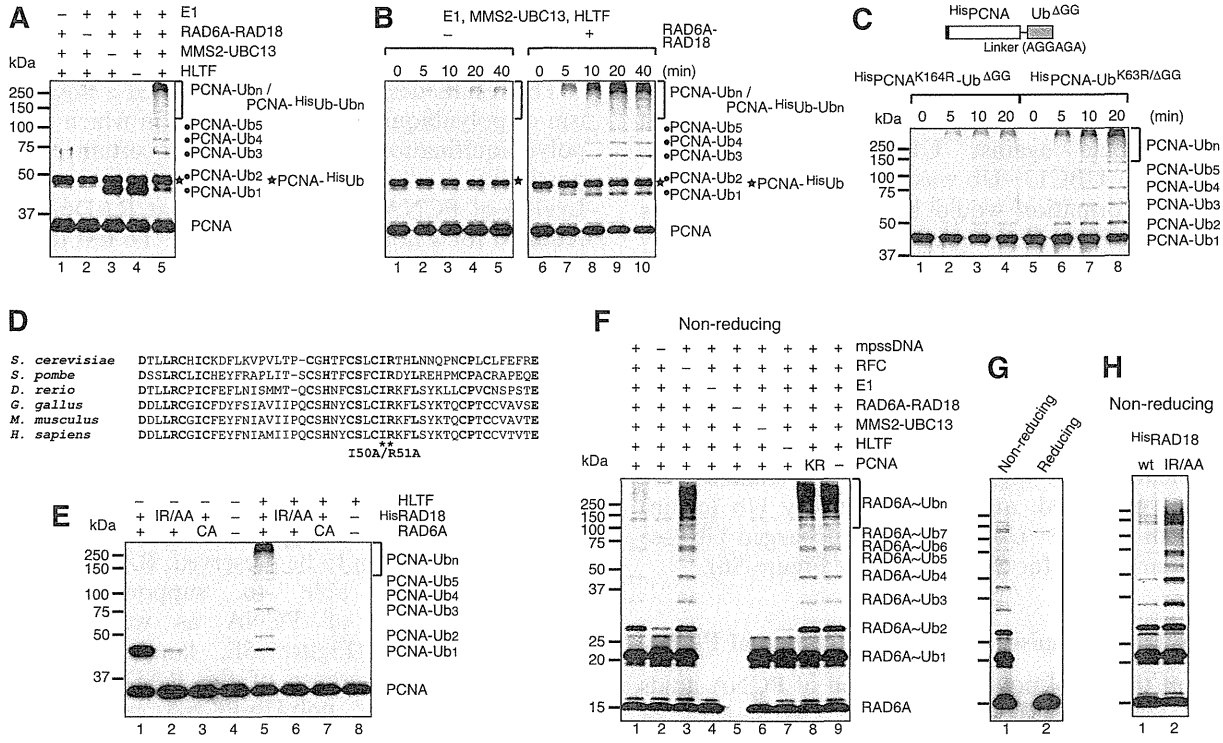

Figure 5. Thiol-linked Ub chains formed on RAD6 are transferred onto PCNA. (**A** and **B**) MonoUb-PCNA is a poor substrate for polyubiquitination. PCNA partially monoubiquitinated with ^{His}Ub was subjected under standard reaction conditions. Reaction products were analyzed by immunoblot using an anti-PCNA antibody. –, omitted factor. (**C**) PCNA ubiquitination assays using ^{His}PCNA–Ub$^{\Delta GG}$ fusion proteins. A schematic of the structure of the fusion protein is shown in the top panel. Reactions were performed with either ^{His}PCNA^{K164R}-Ub$^{\Delta GG}$ or ^{His}PCNA–Ub$^{K63R/\Delta GG}$ instead of PCNA under standard reaction conditions with mpssDNA, RFC, E1, RAD6A–RAD18, MMS2–UBC13, HLTF and Ub, followed by immunoblot using an anti-PCNA antibody. (**D**) Multiple sequence alignment of the RING fingers of human RAD18 and its orthologs. The conserved isoleucine and arginine residues were both replaced with alanines. (**E**) The catalytic activity of RAD6A–RAD18 is required for PCNA polyubiquitination. The reactions were performed using the indicated mutant proteins instead of wild-type protein under standard reaction conditions followed by immunoblot using an anti-PCNA antibody. –, omitted factor; IR/AA, ^{His}RAD18$^{I50A/R51A}$; CA, RAD6A^{C88A}. (**F** and **G**) Ub chain formation on RAD6. The reaction products in Figure 1G and 1H, respectively, were analyzed by immunoblot using an anti-RAD6 antibody. (**H**) Accumulation of RAD6A~Ub$_n$ in complex with the RING mutant of RAD18, RAD18$^{IR/AA}$. The products in lanes 5 and 6 in (E) untreated by a reducing agent were analyzed by immunoblot using an anti-RAD6 antibody (lanes 1 and 2, respectively).

the putative molecular mechanism in more detail. As shown in Figure 6A, RAD6A~Ub$_n$ formation was successfully reconstituted without RFC and PCNA, but was abolished by omission of HLTF, MMS2–UBC13, E1, Ub, mpssDNA or RAD6A–RAD18, which provided additional evidence that these factors are the minimal set of reaction components needed. We confirmed that the multiple bands were Lys63-linked Ub chains on RAD6A by replacing Ub with either ^{FLAG}Ub or Ub^{K63R} (Figure 6B). Furthermore, RAD6A~Ub$_n$ formation was dependent on the catalytic cysteines of UBC13 and RAD6A (Figure 6C, lanes 6 and 7). RAD18 was also an essential component for chain formation (Figure 6C, lane 4), but the RAD18 RING mutant (I50A/R51A) also supported the reaction equally well (Figure 6C, lane 5). Since the RAD18 RING mutant has severely reduced ligase activity in mediating PCNA ubiquitination (Figure 5E) (21), it seems likely that a non-catalytic function of RAD18 other than its ligase activity is required for chain formation on RAD6A. The requirement for the RAD18 subunit might involve a physical interaction between RAD18 and HLTF, as reported previously (11,13). By contrast, the intact RING domain of HLTF was essential for RAD6-Ub$_n$ formation (Figure 6C, lane 3), which indicated that HLTF catalyzes the transfer of Ub molecules from UBC13 to RAD6A.

The formation of RAD6~Ub$_n$ may involve an aminolysis-based transfer reaction between RAD6~Ub and UBC13~Ub$_{n-1}$ (as illustrated in Figure 6D), similar to the mechanism of Ub transfer between UBC13~Ub molecules, as both of the reactions were dependent on the catalytic function of HLTF. In this case, the resulting Ub chain would be expected to be a hybrid between the Ub molecule originally attached to RAD6 and other Ub moieties transferred from UBC13~Ub$_{n-1}$. To investigate the Ub transfer reaction from UBC13~Ub to RAD6~Ub, RAD6A in complex with RAD18 was charged with either ^{His}Ub or ^{His}Ub^{K63R}, and then the modified RAD6A–RAD18 complexes were purified by column chromatography (Figure 6E). The purified complexes supported monoubiquitination of PCNA in the absence of E1 and Ub (Figure 6F), with concomitant reduction in the amount of RAD6A~^{His}Ub and RAD6A~^{His}Ub^{K63R} (Figure 6G). These complexes were then used to test Ub chain formation on RAD6A upon the addition of HLTF and other factors, together with un-tagged Ub^{K63R}, which

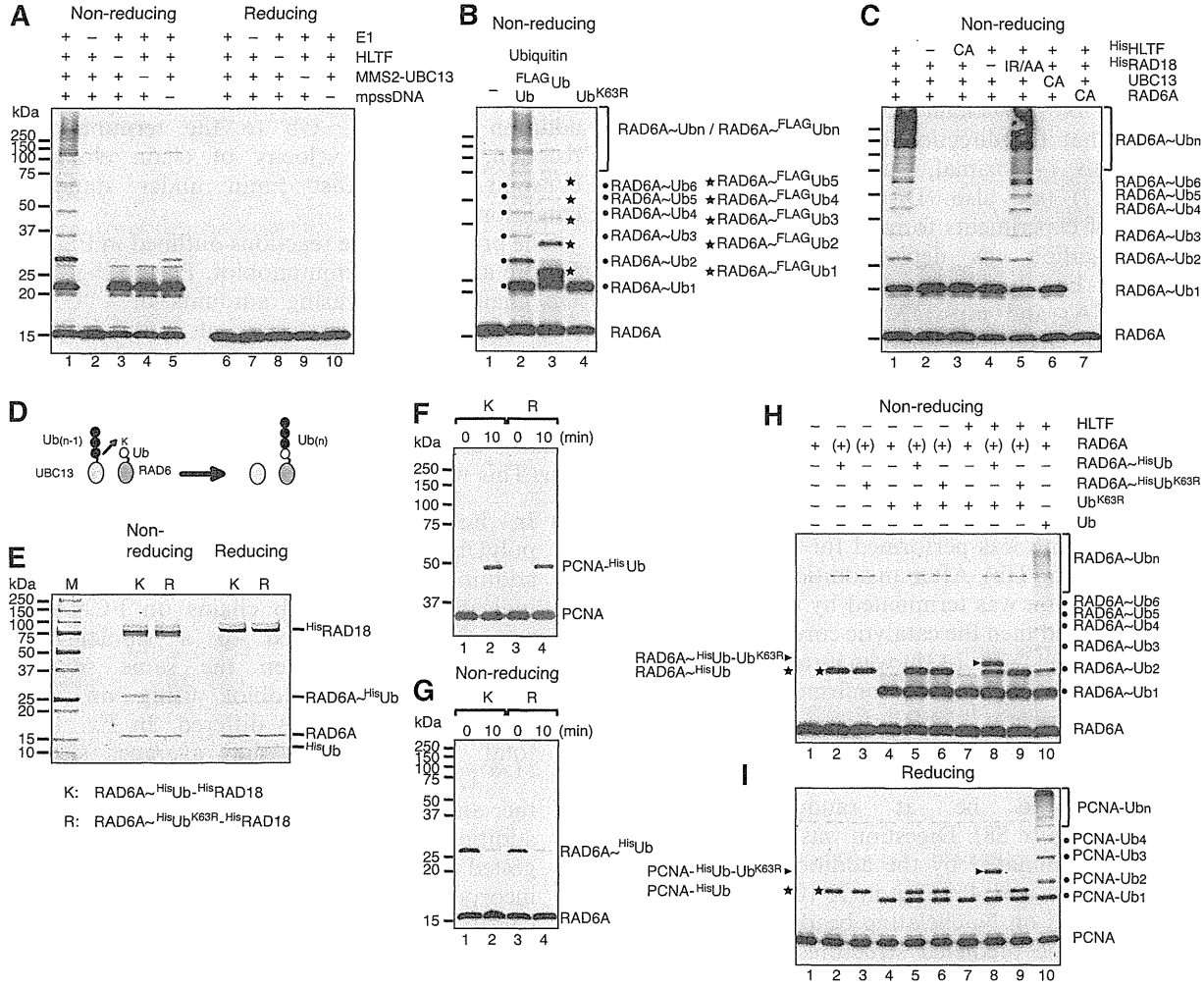

Figure 6. Analysis of RAD6A~Ub_n formation. (**A**) Formation of thiol-linked Ub chains on RAD6A using the minimal set of factors. The reactions were reconstituted with mpssDNA, E1, RAD6A–RAD18, MMS2–UBC13, HLTF and Ub. Reaction products were treated with or without a reducing agent and then analyzed by immunoblot using an anti-RAD6 antibody. –, omitted factor. (**B**) Evidence that the multiple thiol-linked bands on RAD6A are Lys63 linked Ub chains. Reaction products untreated by a reducing agent were analyzed by immunoblot using an anti-RAD6 antibody. The positions of RAD6A~Ub_n and RAD6A~$^{FLAG}Ub_n$ are indicated by dots and stars, respectively. (**C**) Effect of mutants on thiol-linked Ub chain formation on RAD6A. Reaction products untreated by a reducing agent were analyzed by immunoblot using an anti-RAD6 antibody. –, omitted factor; CA for ^{His}HLTF, ^{His}HLTF^{C760A}; IRAA, ^{His}RAD18$^{I50A/R51A}$; CA for UBC13, UBC13^{C87A}; CA for RAD6A and RAD6A^{C88A}. (**D**) Proposed mechanism of RAD6A~Ub_n formation. A red arrow depicts the direction of Ub_n movement. MMS2 and RAD18 were included in the reactions but omitted from the schematic. (**E**) Purified RAD6A~^{His}Ub–^{His}RAD18 and RAD6A~$^{His}Ub^{K63R}$–^{His}RAD18 complexes treated with or without a reducing agent were analyzed by SDS–PAGE followed by CBB staining. (**F** and **G**) PCNA monoubiquitination reactions were reconstituted with PCNA, mpssDNA, RFC and the indicated complexes (K, RAD6A~^{His}Ub–^{His}RAD18; or R, RAD6A~$^{His}Ub^{K63R}$–^{His}RAD18) for the indicated times. Reaction products treated with (F) or without (G) a reducing agent were analyzed by immunoblot using an anti-PCNA antibody (F) or an anti-RAD6 antibody (G). (**H**) Analysis of the Ub transfer reaction from UBC13~Ub to RAD6~Ub. Reactions were performed with mpssDNA, E1, MMS2–UBC13, HLTF, Ub^{K63R}, and either RAD6–^{His}RAD18, RAD6A~^{His}Ub–^{His}RAD18, or RAD6A~$^{His}Ub^{K63R}$–^{His}RAD18 for 2 min. RAD6 molecules shown by (+) were carried from partial charging reactions, as shown in (E). Reaction products untreated with a reducing agent were analyzed by immunoblot using an anti-RAD6 antibody. Lane 10, standard reaction products. (**I**) Analysis of the Ub chain transfer reaction from RAD6~Ub_2 to PCNA. Reactions were performed with PCNA, mpssDNA, RFC, E1, MMS2–UBC13, HLTF, Ub^{K63R}, and either RAD6–^{His}RAD18, RAD6~^{His}Ub–^{His}RAD18, or RAD6~$^{His}Ub^{K63R}$–^{His}RAD18 for 2 min and then analyzed by immunoblot using an anti-PCNA antibody. Lane 10, standard reaction products.

could be distinguished in size from pre-charged ^{His}Ub. If the expected reactions occurred, Ub^{K63R} would be attached to RAD6~^{His}Ub, but not to RAD6A~$^{His}Ub^{K63R}$. As shown in Figure 6H, the formation of an additional band was detected in reactions containing RAD6A~^{His}Ub (lane 8), but not RAD6A~$^{His}Ub^{K63R}$ (lane 9), or uncharged RAD6A (lane 7), and the formation was dependent on HLTF (compare lanes 5 and 8). Importantly, this new band migrated between RAD6A~Ub_2 and RAD6A~Ub_3 (see lane 10), which indicated that it was indeed a RAD6A~^{His}Ub–Ub^{K63R} hybrid. Finally, as shown in Figure 6I, the hybrid chain was transferred onto PCNA to generate PCNA-^{His}Ub–Ub^{K63R} (lane 8), which migrated between PCNA-Ub_2 and PCNA-Ub_3 (see lane 10).

The direction of Ub chain elongation in the PCNA polyubiquitination reaction

The results obtained thus far were consistent with a 'seesaw' model of Ub chain elongation (27), which would predict that the direction of chain elongation is PCNA-distal to -proximal, as hypothesized by Hochstrasser (27) (see also 'Discussion' section). We designed a set of experiments to investigate the direction of chain elongation, as depicted schematically in Figure 7A. In Ex. 1, HLTF, RFC, histidine-tagged PCNA (^{His}PCNA) and mpssDNA were pre-incubated for 2 min and then combined with pre-charged UBC13~Ub. The pre-charging reaction was performed for 2 min with E1, MMS2–UBC13 and Ub. After an initial chain elongation reaction for 1 min, the mixture was combined with pre-charged UBC13~^{FLAG}Ub and then incubated for an additional 1 min. The mixture was then combined with pre-charged RAD6A~Ub with RAD18 (pre-charging was performed for 2 min with E1, RAD6A–RAD18 and Ub). After an additional incubation for 1 min, the reaction was terminated by the addition of EDTA for 1 min, and then the catalytic core of Ub-specific protease 2 [^{His}USP2$^{(258-605)}$] (31) was introduced to partially digest the Ub chains. We confirmed that, unlike isopeptidase T, purified ^{His}USP2$^{(258-605)}$ did not react with terminal Ub moieties of K63-linked Ub chains; rather, the ^{His}USP2$^{(258-605)}$ digestion sites on the Ub chain appeared to be at random positions (Supplementary Figure S8). Digestion was performed for 1 min and then terminated by the addition of an equal volume of 8 M urea and 4% Triton X-100. PCNA was immediately purified on Ni-chelating beads and analyzed by immunoblot. The predicted structures of the major products produced by the three different mechanisms of chain elongation are illustrated in Figure 7A. Note that Ub chain elongation reactions were initiated without ^{FLAG}Ub, and the chains were further extended in presence of ^{FLAG}Ub. If chain elongation occurred via a sequential mechanism, Ub and ^{FLAG}Ub would be incorporated onto PCNA at random, because chain elongation would be initiated by the addition of RAD6A–RAD18 in the presence of both UBC13~Ub and UBC13~^{FLAG}Ub. In the case of *en bloc* transfer, there would be differential distribution of Ub and ^{FLAG}Ub within the chain: accumulation of ^{FLAG}Ub at the PCNA-distal end in the case of sequential addition, and accumulation of ^{FLAG}Ub at the PCNA-proximal end in the case of the seesaw mechanism of addition. In experimental scheme Ex. 2 (Figure 7B), the reactions were the same as Ex. 1, except for the order of the addition of UBC13~Ub and UBC13~^{FLAG}Ub. In Ex. 2, pre-charged UBC13~^{FLAG}Ub was incubated first with HLTF, and then pre-charged UBC13~Ub was added. In Ex. 2, sequential chain elongation would result in the incorporation of Ub and ^{FLAG}Ub onto PCNA in a similar fashion as in Ex. 1. In the case of *en bloc* transfer, the pattern of incorporation of Ub and ^{FLAG}Ub would be the opposite of that depicted in Ex. 1. Note that the distribution of each intermediate varies depending on which molecule is the rate-limiting factor for chain elongation. This also means that if the rate-limiting factor in each step of the overall reaction was altered during incubation, the effects would be significant. To avoid this complication, the experiments were completed within 5 min from the first addition of UBC13~Ub to the termination of the reaction, since the velocity of chain elongation was constant for at least 5 min under standard assay conditions.

The products of the reactions outlined in Figure 7A and B were analyzed by immunoblot. Partial digestion of the Ub chains by increasing amounts of ^{His}USP2$^{(258-605)}$ reduced the average sizes of polyUb-PCNA and produced several distinct bands (Figure 7C). Importantly, the band patterns differed between Ex. 1 and 2 (Figure 7C and D), which suggested that the chains were formed predominantly via a seesaw mechanism. This was supported be the following observations:

(1) In both Ex. 1 and 2, the average sizes of polyUb-PCNA were similarly reduced by the addition of ^{His}USP2$^{(258-605)}$ (Figure 7C), which indicated that the Ub chains on PCNA in Ex. 1 and 2 were digested to a similar extent by ^{His}USP2$^{(258-605)}$. When the same samples were analyzed by immunoblot using an anti-FLAG antibody, the patterns differed. In Ex. 1, both the total amount and the average size of the ^{FLAG}Ub-containing chains (detectable by the anti-FLAG antibody) were decreased by the addition of ^{His}USP2$^{(258-605)}$ (Figure 7D), which suggested that a significant fraction of ^{FLAG}Ub had been incorporated into the PCNA-proximal side. By contrast, in Ex. 2, the average size of the ^{FLAG}Ub-containing chains was only slightly decreased, even though signal intensity was clearly reduced (Figure7D). These results indicated that PCNA containing smaller chains as a result of digestion was no longer detectable with the anti-FLAG antibody, suggesting that ^{FLAG}Ub was predominantly incorporated into the PCNA-distal side.
(2) There was substantial accumulation of ^{FLAG}Ub-free bands, indicated by dots, in Ex. 2 (Figure 7C). By contrast, in Ex.1, ^{FLAG}Ub-containing bands were abundant (Figure 7C and D, stars) even after partial digestion, which suggested that a significant fraction of ^{FLAG}Ub was present on the PCNA-proximal side.

These results were consistent with the pattern predicted by a mechanism of *en bloc* transfer of chains formed by the seesaw mechanism of addition (Figure 8B). Collectively, the results of the current study suggest that the seesaw mechanism predominates in PCNA polyubiquitination reactions.

DISCUSSION

Using an *in vitro* ubiquitination reaction system, we were able to obtain detailed information about the mechanism of PCNA polyubiquitination. Although we cannot exclude the possibility that the reaction conditions were

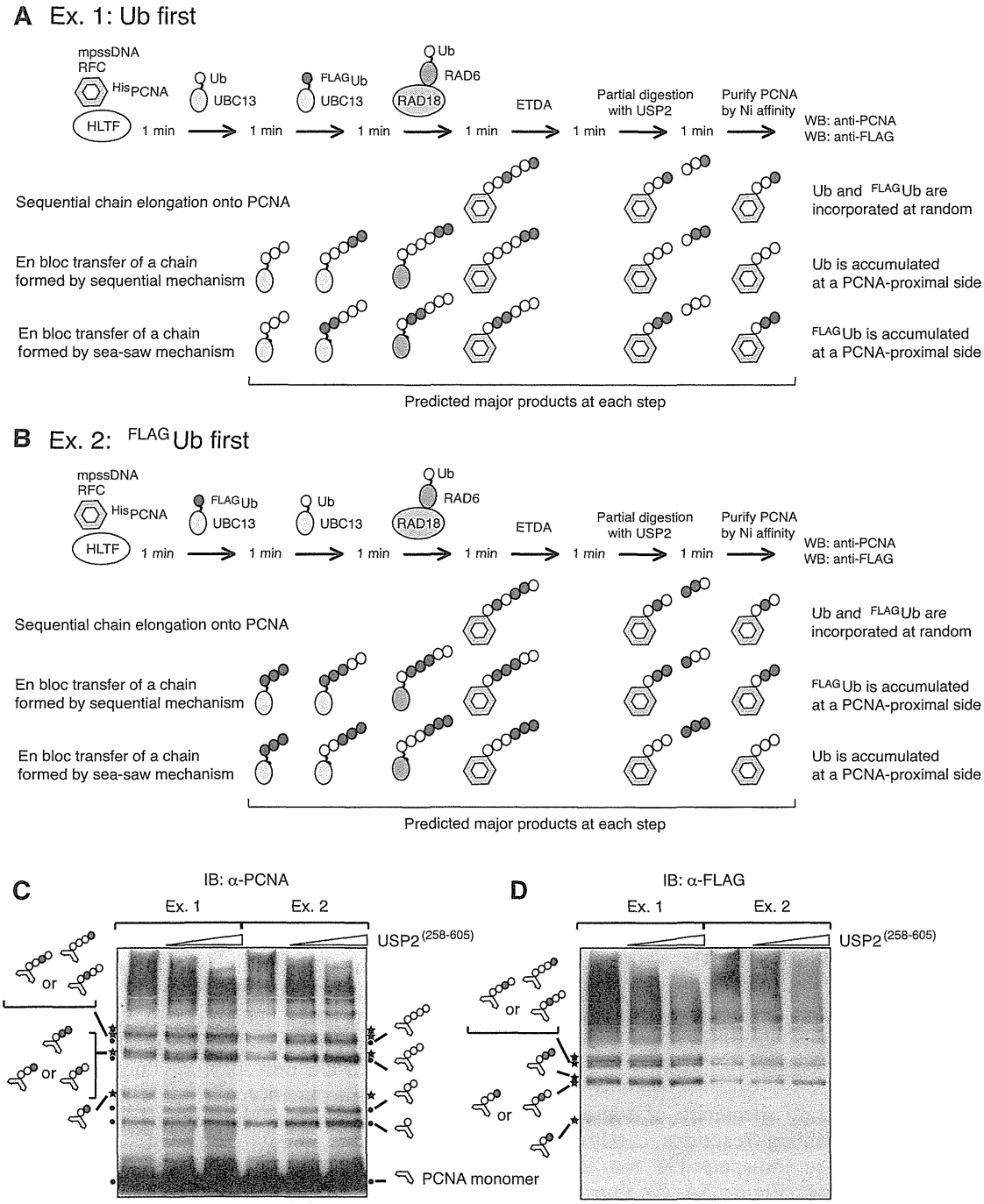

Figure 7. Analysis of the direction of Ub chain elongation. (**A** and **B**) Experimental schemes (see text for details). MMS2 was included in the reactions but omitted from the schematics. (**C** and **D**) Immuonblot analysis using an anti-PCNA antibody to detect total product (C) and an anti-FLAG antibody to detect only ^{FLAG}Ub-containing chains (D). Products containing ^{FLAG}Ub (detected by both the anti-PCNA and anti-FLAG antibodies) are indicated by stars and illustrations. ^{FLAG}Ub-free products (detected by only the anti-PCNA antibody) are indicated by dots and illustrations.

not properly optimized for certain reactions, our results support a novel mechanism of PCNA polyubiquitination that is distinct from, and much more efficient than, the sequential addition reactions of PCNA mono-ubiquitination (Figure 8A) (1,16,17). The mechanism involves pre-formation of a thiol-linked Ub chain on UBC13 and then transfer to RAD6~Ub by HLTF. In this mechanism, HLTF functions as a novel E3 ligase that catalyzes Ub (chain) transfer from UBC13 to the Ub moieties of either UBC13~Ub or RAD6~Ub. This is in contrast to the target protein-specific E3 ligase activity of RAD18, which catalyzes the transfer of Ub chains, as well as Ub monomers, from RAD6 to Lys164 of PCNA. HLTF was also able to catalyze the addition of Ub onto monoUb-PCNA, as described in the sequential addition model, but this activity appeared to be extremely

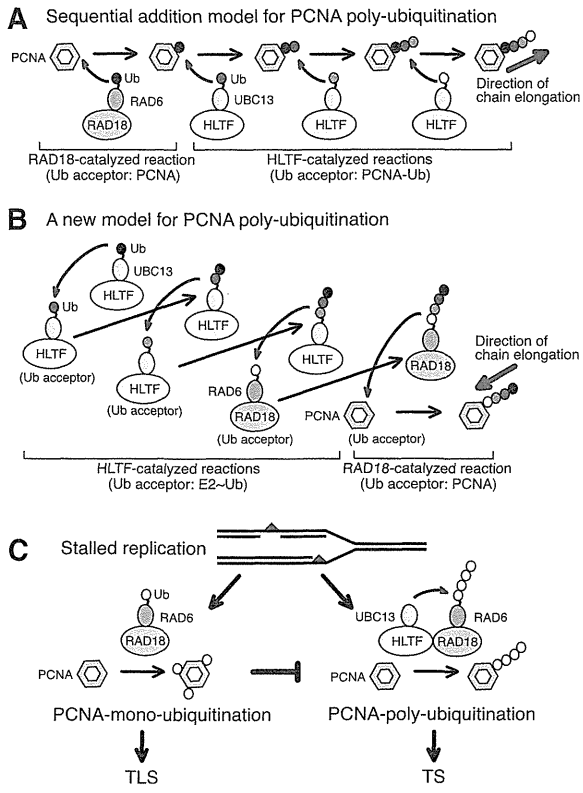

Figure 8. Molecular mechanism of PCNA ubiquitination and implications for the regulation of post-replication repair. MMS2 was omitted to simplify the schematics. A model with MMS2 is shown in Supplementary Figure S9. (**A**) Sequential addition model. RAD18 transfers Ub from RAD6 to PCNA and then HLTF transfers Ub from UBC13 to the terminal Ub moiety of ubiquitinated PCNA. In this model, the Ub chain is elongated in the PCNA-proximal to -distal direction. (**B**) One of potential mechanisms of *en bloc* Ub chain transfer. HLTF transfers Ub from UBC13 to the Ub moiety of UBC13~Ub, generating UBC13~Ub_2. In the next step, the resultant Ub_2 on UBC13 is transferred to the Ub moiety of another UBC13~Ub, generating UBC13~Ub_3. Multiple rounds of this reaction generate long chain UBC13~Ub_n. The Ub chain can be transferred to the Ub moiety of RAD6~Ub, generating RAD6~Ub_{n+1}. RAD18 then transfers the chain from RAD6 to PCNA. In these reactions, the resultant Ub chain has been elongated in the PCNA-distal to -proximal direction. (**C**) Regulation of post-replication repair (see text for details).

low in terms of the substrate specificity of the enzyme (Figure 5A–C). Thus, coupling reactions catalyzed by the two E2–E3 pairs were indispensable for efficient polyubiquitination of PCNA (Figure 5A–C). Our results suggest that HLTF elongates Ub chains via a seesaw type mechanism (27), such that all reactions could be explained by identical biochemical reactions with equivalent substrate specificity. A model is depicted in Figure 8B and Supplementary Figure S9 as one of potential mechanisms of *en bloc* Ub chain transfer. Note that the direction of chain elongation by the seesaw mechanism should be PCNA-distal to -proximal (Figure 8B), which is opposite of that predicted by the conventional model (Figure 8A). This is supported by the data showing that the direction of chain elongation is consistent with a seesaw mechanism of addition (Figure 7).

Our results revealed some interesting properties of HLTF. First, HLTF exhibited a unique specificity for E2~Ub as a substrate. This could represent a biochemical basis for the seesaw mechanism. Second, it functions to regulate Ub chain length. UBC13~Ub_n molecules with long Ub chains ($n \geq 5$) were barely detectable, whereas molecules with short Ub chains ($n \leq 4$) were abundant (Figure 1G). The opposite was observed for RAD6A~Ub_n molecules, with greater accumulation of long chains versus short chains (Figure 5F). These results suggest that the length of the chain attached to UBC13 is enzymatically regulated so that long chains are preferentially transferred to RAD6. Third, DNA was absolutely required for HLTF ligase activity. Since HLTF is a SWI/SNF DNA helicase with a RING domain within the helicase domain, it is likely that the helicase domain is responsible for the interaction with DNA. However, we have been unable to demonstrate a functional interaction between the ligase and helicase domains, as several mutant proteins with alterations in the conserved helicase domain also exhibit ligase activity at levels similar to that of the wild-type protein (Y. Masuda, unpublished data). Previously, it was reported that the Ube2g2 (E2) is capable of producing active site-linked ubiquitin chains with the gp78 (E3), which has been shown to form an oligomer that promotes E2–E2 interactions (32). It is likely that HLTF binding to DNA promotes multimerization of HLTF to stimulate its ligase activity. The precise molecular mechanisms underlying these properties of HLTF remain to be elucidated.

Previously, based on *in vitro* experiments with yRAD5, two groups reported that PCNA polyubiquitination occurs via a conventional, sequential addition reaction mechanism, as depicted in Figure 8A (16,17). The results of these two studies were consistent with some of the genetic studies performed in a *rad18* mutant; namely, that expression of a $PCNA^{K164R}$–Ub fusion protein suppressed defects in both the TLS and TS pathways, but expression of $PCNA^{K164R}$-Ub^{K63R} suppressed only the defect in the TLS pathway, suggesting $PCNA^{K164R}$–Ub, but not $PCNA^{K164R}$–Ub^{K63R}, is polyubiquitinated *in vivo* (33). On the other hand, recent results, also from yeast genetic studies (34,35), demonstrated that expression of $PCNA^{K164R}$–Ub only partially suppresses the *rad18* and *rhp18* mutant phenotype in budding and fission yeast, respectively. In this recent set of studies, $PCNA^{K164R}$–Ub was unable to activate the TS pathway, and this was attributed to the failure to polyubiquitinate the fusion protein. Indeed, $PCNA^{K164R}$–Ub was not polyubiquitinated in either type of yeast (34,35). While these discrepancies in yeast genetic data from different laboratories remain to be resolved, our *in vitro* results are consistent with the more recent genetic data, in that neither $PCNA^{K164R}$–Ub nor monoUb-PCNA was a primary target for polyubiquitination (Figure 5A–C). To directly probe the yRAD5 reaction mechanism, histidine-tagged yRAD5 (^{His}yRAD5) was overexpressed in *E. coli* and partially purified, and then used in our assay system instead of HLTF (Supplementary Figure S6). We expected yRAD5 to interact with the human proteins since HLTF is able to complement the UV sensitivity of a *rad5Δ* strain (13). Indeed, polyubiquitinated PCNA was detected in reactions using partially purified

^{His}yRAD5 (Supplementary Figure S6A). Analysis of the time course of the reaction showed that all of the reaction products, including intermediates, accumulated over time (Supplementary Figure S6B), similar to what was seen with low concentrations of HLTF (Supplementary Figure S2D). Furthermore, monoubiquitinated PCNA was a poor substrate for yRAD5 (Supplementary Figure S6C), similar to that observed for HLTF (Figure 5A). These results suggested that PCNA polyubiquitination by yRAD5 occurs predominantly by *en bloc* transfer of an Ub chain. In the previously reported *in vitro* studies with yRad5, the experiments were for the most part carried out in the absence of RAD6–RAD18, using monoUb-PCNA and either PCNA–Ub fusion proteins (16) or chemically Ub-modified PCNA (17). Even in the presence of RAD6–RAD18, mono- and polyubiquitination were relatively inefficient due to the low activity of RAD6–RAD18 for monoubiquitination (16). Notably, in these studies, the experimental system was designed to detect Ub transfer to monoUb-PCNA. Under similarly uncoupled reaction conditions (i.e. in the absence of RAD6A–RAD18), we were also able to detect Ub transfer to monoUb-PCNA (Figure 5A, lane 2; 5B, lanes 1–5; and 5C, lanes 1–4). The discrepancies between the previous *in vitro* yRad5 studies and the present study are mostly likely due to differences in such reaction conditions. Importantly, however, although the reaction mechanism we defined is completely different from the conventional model, it is essentially consistent with the genetic data; namely both mono- and polyubiquitination are abrogated by inactivation or deletion of either yRAD6 or yRAD18, whereas in the presence of dysfunctional yMMS2, yUBC13, or yRAD5, only polyubiquitination is abrogated (1,2).

If the reaction mechanism we observed *in vitro* mimics what occurs *in vivo*, monoubiquitination and polyubiquitination of PCNA at stalled replication ends would necessarily be promoted separately (Figure 8C). It should be noted that Ub chain formation by UBC13–MMS2 and HLTF required mpssDNA, which differs from the requirement of RAD6–RAD18 for RFC-mediated loading of PCNA on mpssDNA (6,7,36). We hypothesize that PCNA polyubiquitination and activation of the TS pathway is promoted under conditions in which RAD18 and HLTF are coordinately recruited to stalled replication ends, wherein DNA is needed to hold PCNA at the primer terminus (7) and to stimulate HLTF activity. Alternatively, if all three subunits of PCNA at a stalled end are first monoubiquitinated, polyubiquitination cannot occur and the TLS pathway is activated. We have observed that all three subunits of PCNA are efficiently monoubiquitinated at stalled primer ends *in vitro* (7). This scenario could explain how either the TLS or TS pathway is selectively activated at stalled replication sites. The TS pathway would be activated only when a daughter strand that was replicated from the non-damaged parental strand is available and prohibited when such a daughter strand is unavailable. This model is consistent with recent observations from our laboratory that RAD6–RAD18 forms a ternary complex of RAD6A–$(RAD18)_2$ rather than (RAD6A–$RAD18)_2$ and that stable association between RAD6A and RAD18 is an essential requirement for ligase activity (21). These properties of the RAD6–RAD18 complex appear suited for the tight regulation of polyubiquitination of PCNA. If the complex contained two RAD6 molecules, one would have to invoke yet another mechanism involving processive formation of Ub chains on both subunits. Furthermore, if the interaction of RAD6 was dynamic, exchange reactions between RAD6~Ub_n and RAD6~Ub would occur in solution before transfer of the chain to PCNA. The tight regulation of polyubiquitination ensures the timely and appropriate activation of the TS pathway, thereby avoiding irregular recombination. In this manner, eukaryotic cells ensure accurate chromosomal duplication and avoid genetic aberrations that can lead to carcinogenesis.

Finally, we should mention that the seesaw mechanism of ubiquitin chain transfer is similar to the peptidyl transfer reaction of protein synthesis. Conceivably, the concept might be applicable to other E2 and E3 enzymes and another bio-macromolecule synthesis such as oligosaccharides, and may represent a common strategy for the generation of bio-macro-polymers.

SUPPLEMENTARY DATA

Supplementary Data are available at NAR Online: Supplementary Figures 1–10 and Supplementary Notes.

ACKNOWLEDGEMENTS

The authors thank Dr. Toshiki Tsurimoto (Kyushu University, Fukuoka, Japan) for a PCNA-expression plasmid. The authors would also like to express our appreciation to Drs Mark Hochstrasser (Yale University, USA), Haruo Ohmori (Kyoto University, Kyoto, Japan), Richard D. Wood (University of Texas, USA) and Roger Woodgate (NIH, USA) for their comments and suggestions on the manuscript. The authors are furthermore grateful to Yumiko Shintani for making mutants, and Mayumi Hojo, Fumie Okubo, Kazumi Shimamoto, Reiko Tashiro and Mai Yoshida for their laboratory assistance.

FUNDING

Grants-in-Aid from the Ministry of Education, Culture, Sports, Science and Technology of Japan (to Y.M., H.K., H.H., C.M. T.H. and K.K.); Health and Labour Science Research Grants of Japan (to K.K.); the Mitsubishi Foundation and Takeda Science Foundation (to C.M.). Funding for open access charge: JSPS KAKENHI [24310040 to Y.M.].

Conflict of interest statement. None declared.

REFERENCES

1. Friedberg,E.C., Walker,G.C., Siede,W., Wood,R.D., Schultz,R.A. and Ellenberger,T. (2006) *DNA Repair and Mutagenesis*, 2 edn. ASM, Washington, DC.

2. Hoege,C., Pfander,B., Moldovan,G.L., Pyrowolakis,G. and Jentsch,S. (2002) RAD6-dependent DNA repair is linked to modification of PCNA by ubiquitin and SUMO. *Nature*, **419**, 135–141.
3. Kannouche,P.L., Wing,J. and Lehmann,A.R. (2004) Interaction of human DNA polymerase η with monoubiquitinated PCNA: a possible mechanism for the polymerase switch in response to DNA damage. *Mol. Cell*, **14**, 491–500.
4. Watanabe,K., Tateishi,S., Kawasuji,M., Tsurimoto,T., Inoue,H. and Yamaizumi,M. (2004) Rad18 guides polη to replication stalling sites through physical interaction and PCNA monoubiquitination. *EMBO J.*, **23**, 3886–3896.
5. Bienko,M., Green,C.M., Crosetto,N., Rudolf,F., Zapart,G., Coull,B., Kannouche,P., Wider,G., Peter,M., Lehmann,A.R. *et al.* (2005) Ubiquitin-binding domains in Y-family polymerases regulate translesion synthesis. *Science*, **310**, 1821–1824.
6. Garg,P. and Burgers,P.M. (2005) Ubiquitinated proliferating cell nuclear antigen activates translesion DNA polymerases η and REV1. *Proc. Natl Acad. Sci. USA*, **102**, 18361–18366.
7. Masuda,Y., Piao,J. and Kamiya,K. (2010) DNA replication-coupled PCNA mono-ubiquitination and polymerase switching in a human *in vitro* system. *J. Mol. Biol.*, **396**, 487–500.
8. Wood,A., Garg,P. and Burgers,P.M. (2007) A ubiquitin-binding motif in the translesion DNA polymerase Rev1 mediates its essential functional interaction with ubiquitinated proliferating cell nuclear antigen in response to DNA damage. *J. Biol. Chem.*, **282**, 20256–20263.
9. Zhuang,Z., Johnson,R.E., Haracska,L., Prakash,L., Prakash,S. and Benkovic,S.J. (2008) Regulation of polymerase exchange between Polη and Polδ by monoubiquitination of PCNA and the movement of DNA polymerase holoenzyme. *Proc. Natl Acad. Sci. USA*, **105**, 5361–5366.
10. MacKay,C., Toth,R. and Rouse,J. (2009) Biochemical characterisation of the SWI/SNF family member HLTF. *Biochem. Biophys. Res. Commun.*, **390**, 187–191.
11. Motegi,A., Liaw,H.J., Lee,K.Y., Roest,H.P., Maas,A., Wu,X., Moinova,H., Markowitz,S.D., Ding,H., Hoeijmakers,J.H. *et al.* (2008) Polyubiquitination of proliferating cell nuclear antigen by HLTF and SHPRH prevents genomic instability from stalled replication forks. *Proc. Natl Acad. Sci. USA*, **105**, 12411–12416.
12. Motegi,A., Sood,R., Moinova,H., Markowitz,S.D., Liu,P.P. and Myung,K. (2006) Human SHPRH suppresses genomic instability through proliferating cell nuclear antigen polyubiquitination. *J. Cell. Biol.*, **175**, 703–708.
13. Unk,I., Hajdu,I., Fatyol,K., Hurwitz,J., Yoon,J.H., Prakash,L., Prakash,S. and Haracska,L. (2008) Human HLTF functions as a ubiquitin ligase for proliferating cell nuclear antigen polyubiquitination. *Proc. Natl Acad. Sci. USA*, **105**, 3768–3773.
14. Unk,I., Hajdu,I., Fatyol,K., Szakal,B., Blastyak,A., Bermudez,V., Hurwitz,J., Prakash,L., Prakash,S. and Haracska,L. (2006) Human SHPRH is a ubiquitin ligase for Mms2-Ubc13-dependent polyubiquitylation of proliferating cell nuclear antigen. *Proc. Natl Acad. Sci. USA*, **103**, 18107–18112.
15. Hofmann,R.M. and Pickart,C.M. (1999) Noncanonical MMS2-encoded ubiquitin-conjugating enzyme functions in assembly of novel polyubiquitin chains for DNA repair. *Cell*, **96**, 645–653.
16. Parker,J.L. and Ulrich,H.D. (2009) Mechanistic analysis of PCNA poly-ubiquitylation by the ubiquitin protein ligases Rad18 and Rad5. *EMBO J.*, **28**, 3657–3666.
17. Carlile,C.M., Pickart,C.M., Matunis,M.J. and Cohen,R.E. (2009) Synthesis of free and proliferating cell nuclear antigen-bound polyubiquitin chains by the RING E3 ubiquitin ligase Rad5. *J. Biol. Chem.*, **284**, 29326–29334.
18. Fukuda,K., Morioka,H., Imajou,S., Ikeda,S., Ohtsuka,E. and Tsurimoto,T. (1995) Structure-function relationship of the eukaryotic DNA replication factor, proliferating cell nuclear antigen. *J. Biol. Chem.*, **270**, 22527–22534.
19. Masuda,Y., Suzuki,M., Piao,J., Gu,Y., Tsurimoto,T. and Kamiya,K. (2007) Dynamics of human replication factors in the elongation phase of DNA replication. *Nucleic Acids Res.*, **35**, 6904–6916.
20. Tomida,J., Masuda,Y., Hiroaki,H., Ishikawa,T., Song,I., Tsurimoto,T., Tateishi,S., Shiomi,T., Kamei,Y., Kim,J. *et al.* (2008) DNA damage-induced ubiquitylation of RFC2 subunit of replication factor C complex. *J. Biol. Chem.*, **283**, 9071–9079.
21. Masuda,Y., Suzuki,M., Kawai,H., Suzuki,F. and Kamiya,K. (2012) Asymmetric nature of two subunits of RAD18, a RING-type ubiquitin ligase E3, in the human RAD6A-RAD18 ternary complex. *Nucleic Acids Res.*, **40**, 1065–1076.
22. Gu,Y., Masuda,Y. and Kamiya,K. (2008) Biochemical analysis of human PIF1 helicase and functions of its N-terminal domain. *Nucleic Acids Res.*, **36**, 6295–6308.
23. Ecker,D.J., Butt,T.R., Marsh,J., Sternberg,E.J., Margolis,N., Monia,B.P., Jonnalagadda,S., Khan,M.I., Weber,P.L., Mueller,L. *et al.* (1987) Gene synthesis, expression, structures, and functional activities of site-specific mutants of ubiquitin. *J. Biol. Chem.*, **262**, 14213–14221.
24. Haas,A.L. and Rose,I.A. (1982) The mechanism of ubiquitin activating enzyme. A kinetic and equilibrium analysis. *J. Biol. Chem.*, **257**, 10329–10337.
25. Li,W., Tu,D., Brunger,A.T. and Ye,Y. (2007) A ubiquitin ligase transfers preformed polyubiquitin chains from a conjugating enzyme to a substrate. *Nature*, **446**, 333–337.
26. Petroski,M.D. and Deshaies,R.J. (2005) Mechanism of lysine 48-linked ubiquitin-chain synthesis by the cullin-RING ubiquitin-ligase complex SCF-Cdc34. *Cell*, **123**, 1107–1120.
27. Hochstrasser,M. (2006) Lingering mysteries of ubiquitin-chain assembly. *Cell*, **124**, 27–34.
28. Eddins,M.J., Carlile,C.M., Gomez,K.M., Pickart,C.M. and Wolberger,C. (2006) Mms2-Ubc13 covalently bound to ubiquitin reveals the structural basis of linkage-specific polyubiquitin chain formation. *Nat. Struct. Mol. Biol.*, **13**, 915–920.
29. Deshaies,R.J. and Joazeiro,C.A. (2009) RING domain E3 ubiquitin ligases. *Annu. Rev. Biochem.*, **78**, 399–434.
30. Zheng,N., Wang,P., Jeffrey,P.D. and Pavletich,N.P. (2000) Structure of a c-Cbl-UbcH7 complex: RING domain function in ubiquitin-protein ligases. *Cell*, **102**, 533–539.
31. Renatus,M., Parrado,S.G., D'Arcy,A., Eidhoff,U., Gerhartz,B., Hassiepen,U., Pierrat,B., Riedl,R., Vinzenz,D., Worpenberg,S. *et al.* (2006) Structural basis of ubiquitin recognition by the deubiquitinating protease USP2. *Structure*, **14**, 1293–1302.
32. Li,W., Tu,D., Li,L., Wollert,T., Ghirlando,R., Brunger,A.T. and Ye,Y. (2009) Mechanistic insights into active site-associated polyubiquitination by the ubiquitin-conjugating enzyme Ube2g2. *Proc. Natl Acad. Sci. USA*, **106**, 3722–3727.
33. Zhao,S. and Ulrich,H.D. (2010) Distinct consequences of posttranslational modification by linear versus K63-linked polyubiquitin chains. *Proc. Natl Acad. Sci. USA*, **107**, 7704–7709.
34. Pastushok,L., Hanna,M. and Xiao,W. (2010) Constitutive fusion of ubiquitin to PCNA provides DNA damage tolerance independent of translesion polymerase activities. *Nucleic Acids Res.*, **38**, 5047–5058.
35. Ramasubramanyan,S., Coulon,S., Fuchs,R.P., Lehmann,A.R. and Green,C.M. (2010) Ubiquitin-PCNA fusion as a mimic for mono-ubiquitinated PCNA in *Schizosaccharomyces pombe*. *DNA Repair*, **9**, 777–784.
36. Haracska,L., Unk,I., Prakash,L. and Prakash,S. (2006) Ubiquitylation of yeast proliferating cell nuclear antigen and its implications for translesion DNA synthesis. *Proc. Natl Acad. Sci. USA*, **103**, 6477–6482.

Journal of Cellular Physiology

Hyperthermia Inhibits Homologous Recombination Repair and Sensitizes Cells to Ionizing Radiation in a Time- and Temperature-Dependent Manner

STEFAN C. GENET,[1] YOSHIHIRO FUJII,[2] JUNKO MAEDA,[1] MASAMI KANEKO,[1] MATTHEW D. GENET,[1] KIYOSHI MIYAGAWA,[2] AND TAKAMITSU A. KATO[1]*

[1]*Department of Environmental and Radiological Health Sciences, Colorado State University, Fort Collins, Colorado*

[2]*Graduate School of Medicine, University of Tokyo, Tokyo, Japan*

Hyperthermia has long been known as a radio-sensitizing agent that displays anti-tumor effects, and has been developed as a therapeutic application. The mechanisms of hyperthermia-induced radio-sensitization are highly associated with inhibition of DNA repair. Our investigations aimed to show how hyperthermia inactivate homologous recombination repair in the process of sensitizing cells to ionizing radiation by using a series of DNA repair deficient Chinese Hamster cells. Significant differences in cellular toxicity attributable to hyperthermia at and above 42.5°C were observed. In wild-type and non-homologous end joining repair mutants, cells in late S phase showed double the amount heat-induced radio-sensitization effects of G1-phase cells. Both radiation-induced DNA double strand breaks and chromatin damage resulting from hyperthermia exposure was measured to be approximately two times higher in G2-phase cells than G0/G1 cells. Additionally, G2-phase cells took approximately two times as long to repair DNA damage over time than G0/G1-phase cells. To supplement these findings, radiation-induced Rad51 foci formations at DNA double strand break sites were observed to gradually dissociate in response to the temperature and time of hyperthermia exposure. Dissociated Rad51 proteins subsequently re-formed foci at damage sites with time, and occurred in a trend also related to temperature and time of hyperthermia exposure. These findings suggest Rad51's dissociation and subsequent reformation at DNA double strand break sites in response to varying hyperthermia conditions plays an important role in hyperthermia-induced radio-sensitization.

J. Cell. Physiol. 9999: 1–9, 2012.

Hyperthermia is known to act as a radio-sensitizer and to preferentially kill cells that are resistant to radiation alone. These effects have been shown to occur in a time–temperature-dependent manner (Dewey et al., 1977; Dynlacht et al., 2003, 2004). In clinical settings, tissues are typically heated to a temperature of 39–45°C (van der Zee et al., 2008). Hyperthermia alone kills cells in all phases of the cell cycle, but is most effective in selectively killing cells undergoing the process of DNA replication during S phase, a crucial point in the cell cycle where mammalian cells are known to be resistant to the effects of low LET radiation (Westra and Dewey, 1971; Hahn, 1974; Bhuyan, 1979; Rice et al., 1984; Roti Roti, 2007). Furthermore, hyperthermia-induced enhancement of cell killing, when combined with radiation treatment, has been shown to specifically interfere with the *repair* of potentially lethal DNA double strand breaks attributable to radiation exposure (Iliakis and Seaner, 1990; Deorukhakar et al., 1993; Raaphorst et al., 1993, 2004; Nevaldine et al., 1994; Iliakis et al., 2008; Laszlo and Fleischer, 2009; Krawczyk et al., 2011). Its lethal effects have also been associated with increasing amounts of DNA damage within a cell (Mitchel and Birnboims, 1985; Takahashi et al., 2004). The toxic effect hyperthermia has on cells in the process of DNA repair is related to subsequent denaturing of proteins involved in DNA repair due to elevated temperatures within a cell (Roti Roti, 2007). Thus, if a cell's repair mechanisms for double strand breaks are inhibited following exposure to ionizing radiation, double strand breaks remain unrepaired and can lead to cell death. Inhibiting the repair of malignant cell's radiation-inducedDNA double strands breaks is appealing due to the potential to increase tumor control in radiation therapy.

Evidence exists indicating that among the various DNA lesions induced by radiation (i.e., single strand breaks, double strand breaks, base damage, and crosslinking), DNA double strand breaks are the most severe, which tend to result in chromosome fragmentation leading to subsequent cell death if left unrepaired (Iliakis and Seaner, 1990). In mammalian cells, the ability to repair these double strand breaks involve two pathways: non-homologous end joining and homologous recombination. The non-homologous end joining pathway functions in all phases of the cell cycle, whereas homologous recombination primarily functions during late S and G2 phases (Kampinga et al., 2004; Iliakis et al., 2008; San Filippo et al., 2008; Weterings and Chen, 2008). Due to late S phase being one of

Conflict of interest: nothing to declare.

Contract grant sponsor: Colorado State University.
Contract grant sponsor: College Research Council fund from the College of Veterinary Medicine and Biomedical Sciences, Colorado State University.

*Correspondence to: Takamitsu A. Kato, Assistant Professor, Department of Environmental and Radiological Health Sciences, Colorado State University, 1618 Campus Delivery, Fort Collins, CO 80523. E-mail: takamitsu.kato@colostate.edu

Manuscript Received: 16 April 2012
Manuscript Accepted: 28 November 2012

Accepted manuscript online in Wiley Online Library (wileyonlinelibrary.com): 00 Month 2012.
DOI: 10.1002/jcp.24302

the most radiation-resistant phases of the cell cycle, the combination of heat and radiation may be a more effective protocol for radiotherapy pending necessary elucidation of hyperthermia's role in creating and sustaining dysfunction in these DNA repair mechanism responsible for repairing radiation-induced DNA double stand breaks.

Recent studies revealed that hyperthermia leads to annihilation of radiation-induced DNA repair foci such as MRE11, RPA 34, BRCA 2, and Rad51 (Dynlacht et al., 2004; Xu et al., 2007; Krawczyk et al., 2011). These findings have supplemented previous knowledge that heat shock at and above 43°C inhibits repair of DNA damage induced by ionizing radiation (Kampinga et al., 2004). Although several studies have investigated hyperthermia's role in enhancing cell-killing effects when combined with radiation, the controlling factors underlying the quantifiable amount of hyperthermia and radiation's synergistic cellular lethality effects have not been fully understood. In light of recent recognition of hyperthermia abolishing major DNA homologous recombination repair foci, we focused our investigative efforts on varying hyperthermic conditions' interplay with an upstream homologous recombination protein, Rad 51, using several Chinese Hamster Ovary (CHO) cell lines to identify a dependence, if any, on varying hyperthermic conditions leading to the inactivation of homologous recombination repair mechanism.

The primary goals in this study were to determine the main DNA repair mechanistic target of hyperthermic conditions and to subsequently measure the level and time of inhibition in response to varying hyperthermic conditions following radiation exposure. In our investigations, we exposed various DNA-repair deficient cell lines lacking specific protein expression involved with non-homologous end joining or homologous recombination repair derived from CHO cells to hyperthermia alone and hyperthermia/radiation conjunctive treatments. To supplement these hyperthermia-radiation experiments, immunocytochemistry was utilized to observe Rad51 and γ-H2AX foci before, during, and after hyperthermia in CHO wild-type cells. We observed the obliteration and restoration of Rad51 foci at DNA double strand break sites in a time–temperature-dependent manner (while still being detectable in the nucleus and cytoplasm), whereas γ-H2AX foci remained throughout manipulated hyperthermic conditions following a standardized 1 Gy exposure of gamma rays. Our findings highlight the importance of Rad51-mediated homologous recombination DNA repair capacity as well as the importance of time and temperature of heat application in determining cell's response to hyperthermia treatments following radiological insults.

Materials and Methods

Cell culture

CHO WT (CHO 10B2) and AG1521 normal human fibroblast cells were kindly supplied from Dr. Joel Bedford of Colorado State University (Fort Collins, CO, USA). DNA repair deficient CHO mutants, V3 (DNA-PKcs), irs1SF (XRCC3), KO40 (FancG), 51D1 (Rad51D), and xrs5 (Ku80) and V79 mutants irs1 (XRCC2) and irs3 (Rad51C) were kindly supplied along with gene complimented versions of these cells from Dr. Larry Thompson of Lawrence Livermore National Laboratory (Livermore, CA, USA; Tebbs et al., 2005; Hinz et al., 2006). Chinese hamster cells were maintained in Alpha MEM (Hyclone, ThermoFisher, Waltham, MA) with 10% FBS (Sigma, St. Louis, MO), antibiotics (Anti-Anti; Invitrogen, Grand Island, NY) and were cultured in 37°C incubators with 5% CO_2 and humidity. AG1521 cells were cultured in Alpha MEM (Hyclone) with 15% FBS (Sigma), antibiotics and were cultured in 37°C incubators with 5% CO_2 and humidity.

Hyperthermia and radiation conditions

Cells were irradiated with a TITAN X-ray generator (Shimadzu, Tokyo, Japan) using 0.5 mm Al and Cu filters at 200 kVp and 20 mA or a J.L. Shepard Mark I ^{137}Cs 6000Ci Gamma-Ray irradiator (Kato et al., 2008). Dose rate was approximately 1 Gy/min for X-rays and 2.5 Gy/min for gamma rays at room temperature. For hyperthermia, tightly sealed cell culture containers were immersed in a pre-heated temperature controlled water bath (Lauda, ThermoFisher, Waltham, MA) ranging in temperature from 41.5 to 46°C for a time of 10–200 min.

Cell cycle synchronization

Experiments were carried out using cell populations in exponential log phase growth. All CHO cell lines were synchronized in G1-phase or late S-phase using a mitotic shake off method (Tobey and Ley, 1970). After harvesting, suspended mitotic cells were transferred into new culture containers. Flow cytometry analysis confirmed positions within cell cycle.

Synchronized AG1521 cells in G0/G1-phase were produced by contact inhibition. DNA damage in G2-phase cells was identified using exponentially growing populations counter stained by a G2-phase immunocytochemistry marker, CENP-F antibody.

Cell survival colony formation assay

After exposure to radiation, hyperthermia, or a combination of both, cells were trypsinized and plated to form colonies. Colonies were fixed and stained 7–10 days later using 100% ethanol followed by 0.1% crystal violet. Macroscopic colonies containing more than 50 cells (i.e., those formed from seeded cells that did not undergo a mitotic cell death following radiation exposure) were marked as a survivor (Kato et al., 2008).

Thermal enhancement ratio (TER) was calculated from D_{10} values (radiation dose to achieve 10% cell survival). D_{10} values were obtained from Graphpad Prism 5 software (Graph Pad, La Jolla, CA) with linear quadratic regression model. TER = (D_{10} of control sample)/(D_{10} with hyperthermia).

Immunostaining for DNA repair proteins

Following exposure to hyperthermia, cells were fixed in 4% paraformaldehyde for 15 min, immersed in 0.5% Triton X-100 and 0.1% SDS in PBS solution for 10 min. After overnight blocking with 10% goat serum in PBS solution, immunostaining was carried out. Primary antibodies were mouse monoclonal γ-H2AX antibodies (Millipore, Billerica, MA), CENP-F rabbit polyclonal antibodies for G2 DNA damage (Santa Cruz Biotechnology, Santa Cruz, CA) and rabbit polyclonal Rad51 antibodies for homologous recombination analysis (Santa Cruz Biotechnology). Secondary antibodies were Alexa 488-conjugated anti-mouse goat antibodies and Alexa 594-conjugated anti-rabbit goat antibodies (Invitrogen). DNA was counterstained by DAPI with Antifade Gold (Invitrogen). Images were captured and analyzed with an Olympus BX51 fluorescence microscope (Olympus, Tokyo, Japan) and a Q-image Aqua cooled CCD camera (Q-Imaging, Surrey, BC, Canada).

G2 premature chromosome condensation (PCC) assay

Following radiation and hyperthermia treatments, exponentially growing AG1521 cells were treated with 50 nM of Calyculin A (Sigma) for 30 min. Cells were then treated with hypotonic 75 mM KCl solution for 20 min at 37°C. Samples were then fixed in methanol–acetic acid solution (3:1 mixture) three times. Resulting chromosome spreads were prepared on slide glass and stained with 5% filtered Giemsa solution in Gurr (Invitrogen). G2-PCC aberration images were captured and analyzed with an Olympus BX51 brightfield microscope (Olympus) and a DP30 cooled CCD camera (Olympus). Chromatid gaps, breaks, iso-breaks, and exchanges were all scored as chromatid aberrations.

Arrhenius plot calculations

For cell survival data, 1/37% isosurvival values were obtained by taking the inverse of the time value (min) to produce specific survival fractions at a given temperature. Inverse of immunocytochemistry isoeffect values were represented by the inverse of the time (min) value required to reduce the fraction of cells with Rad51/γ-H2AX co-localizations to 37% of background levels (sample of WT cells treated with 1 Gy of gamma rays alone with approximately 50% of cells having co-localizations) at a corresponding temperature. These values were then plotted on the ordinate against their respective temperatures on the abscissa.

Statistics

All experiments were carried out at least three times and error bars indicate standard error of the means. Data were analyzed using Prism 5 software for Student's *t*-test. *P*-values <0.05 were categorized as significant differences.

Results

Log-phase cell survival after hyperthermia

Hyperthermia-induced cell killing was measured via colony formation assay following exposure to various times and temperatures of hyperthermic conditions (Fig. 1A). Homologous recombination mutant cell lines irs1SF and 51D1 and Ku-80 mutant xrs5 were comparably sensitive to hyperthermia exposure at all temperatures relative to non-homologous end joining mutant V3 and wild-type cells. In order to visualize the relative sensitivity to hyperthermia in each cell line, an inverse isosurvival plot consisting of 1/37% survival values plotted against respective temperatures was created to indicate a time- and temperature-dependent change in cell-killing data trend in response to hyperthermic conditions alone (Fig. 1B). We utilized these inverse isosurvival plots to visualize an approximated threshold temperature at which hyperthermia elicits noticeable changes in the time (i.e., dose) to produce a standardized survival fraction for studied discrete temperatures. At temperature ranges of approximately 42.0–42.5°C, decreasing intervals between isosurvival values at discrete time points for temperature doses differing by 0.5°C in the utilized cell lines were observed, particularly in wild-type cells. Due to a pronounced change in isosurvival doses between temperatures of 42.0 and 42.5°C in wild-type cells, we chose to use 42.5°C in our subsequent radiosensitization with hyperthermia and immunostaining assays.

Hyperthermia-induced radio-sensitivities in proliferative and synchronized cells

Hyperthermia-induced radio-sensitization was compared between both non-synchronized and synchronized cell populations via a colony formation assay following radiation alone, or radiation–hyperthermia conjunctive treatments (Fig. 2A). The hyperthermia-induced radio-sensitization was evaluated by TER from D_{10} values. Non-synchronized wild-type (1.67), non-homologous end joining mutant cell lines V3 (1.87), and both mutant/gene complimented versions of the Fanconi Anemia mutant cell line, KO40 (1.65/1.69), showed the most significant level of hyperthermia-related enhancement of cell killing (Fig. 2A). Contrary to these results, non-synchronized homologous recombination mutant cell lines 51D1 (1.06), irs1SF (1.06), irs1 (1.08), and irs3 (1.21) displayed smaller hyperthermia-related enhancement of cell killing. Gene complimented versions of homologous recombination mutant cell lines displayed a hyperthermia-related enhancement of cell killing when compared to their mutant counterparts (1.52, 1.52, and 1.45, respectively, except irs3; Fig. 2A). In regards to synchronized wild-type and V3 cell populations, late S-phase cells displayed the highest level of toxicity related to hyperthermia compared to cells in G1 phase. Homologous recombination mutant cell line 51D1 showed no hyperthermia-related enhancement of cell killing in either G1 or S phase. TERs calculated from D_{10} values for wild-type cells presented as 1.14 (G1) and 2.03 (S), V3 cells presented as 1.45 (G1) and 1.99 (S), and 51D1 cells presented as1.10 (G1) and 0.93 (S; Fig. 2B). This implies that hyperthermia-induced radio-sensitization during this point of the cell cycle is largely dependent on the loss of homologous recombination repair.

G2-premature chromatin condensation (PCC) assay in AG1521 human fibroblast cells

Hyperthermia's effect on G2 phase DNA repair was confirmed by a G2-PCC assay following the aforementioned radiation–hyperthermia exposure experiments. Based on our G2-PCC assay, half-life of chromatid aberrations was approximately 1.1 h for unheated control samples and exposure to hyperthermia resulted in a reduced ability to diminish chromatid aberrations over time post-treatment relative to samples treated with radiation alone. Hyperthermia slows down the kinetics of DNA repair due to higher levels of remaining chromatin damage in cells 3-h post-exposure to both hyperthermia and radiation relative to cells exposed to hyperthermia alone (*t*-test, $P<0.0001$; Fig. 3A).

DNA repair kinetics by γ-H2AX immunostaining in AG1521 human fibroblast cells

Contact-inhibited G0/G1-phase AG1521 cells and G2-phase cells identified by a CENP-F antibody (G2-phase marker) were subjected to a γ-H2AX immunostaining assay every 1.5 h following exposure to 1 Gy of X-rays in order to evaluate levels of DNA repair. G2-phase cells exposed to hyperthermia-radiation conjunctive treatments displayed a reduced ability to diminish DNA double strand breaks over time post-treatment relative to their radiation-alone treated counterparts. Although there were no significant differences at each time point with and without hyperthermia in G0/G1-phases, G2-phase cells showed significantly slower repair in several time points (e.g., the *P*-value was <0.001 at 6 h after radiation exposure). Half-life calculations of remaining γ-H2AX-foci were used to quantify the level of DNA repair activity in the different synchronized cell populations. Half-life calculations (means at 95% confidence intervals) were as follows: G0/G1 control was 2.1 h (1.78–2.52), G0/G1 with heat was 2.0 h (1.42–3.24), G2 control was 1.9 h (1.62–2.28), and G2 with heat was 4.4 h (3.24–6.61). Cells in G0/G1 phases showed a small initial amount of γ-H2AX foci due to smaller target DNA volume. Cells in G2 phase displayed a higher initial amount of γ-H2AX foci, and showed severe hyperthermia effects for DNA repair capability (Fig. 3B).

Rad51/γ-H2AX co-localization assay with immunocytochemistry

Based on the results from cell survival experiments, we speculated that the inactivation of the homologous-recombination repair mechanism involved in repair of DNA double strand breaks during S and G2 phases of the cell cycle plays a key role in hyperthermia-induced radio-sensitization. To test this hypothesis, we observed Rad-51/γ-H2AX co-localizations in CHO wild-type cell populations in a time-progressive manner following radiation–hyperthermia conjunctive treatments (Figs. A and 5). Samples were exposed to 1 Gy of gamma rays, incubated at 37°C for 1 h, then exposed to differing hyperthermic doses of time and temperature. The number of cells with Rad51/γ-H2AX co-localizations out of a given population was scored to quantify co-localization frequencies. Following various hyperthermia treatments, Rad51 foci in these cell populations disappeared in a time- and temperature-dependent manner, but γ-H2AX foci remained

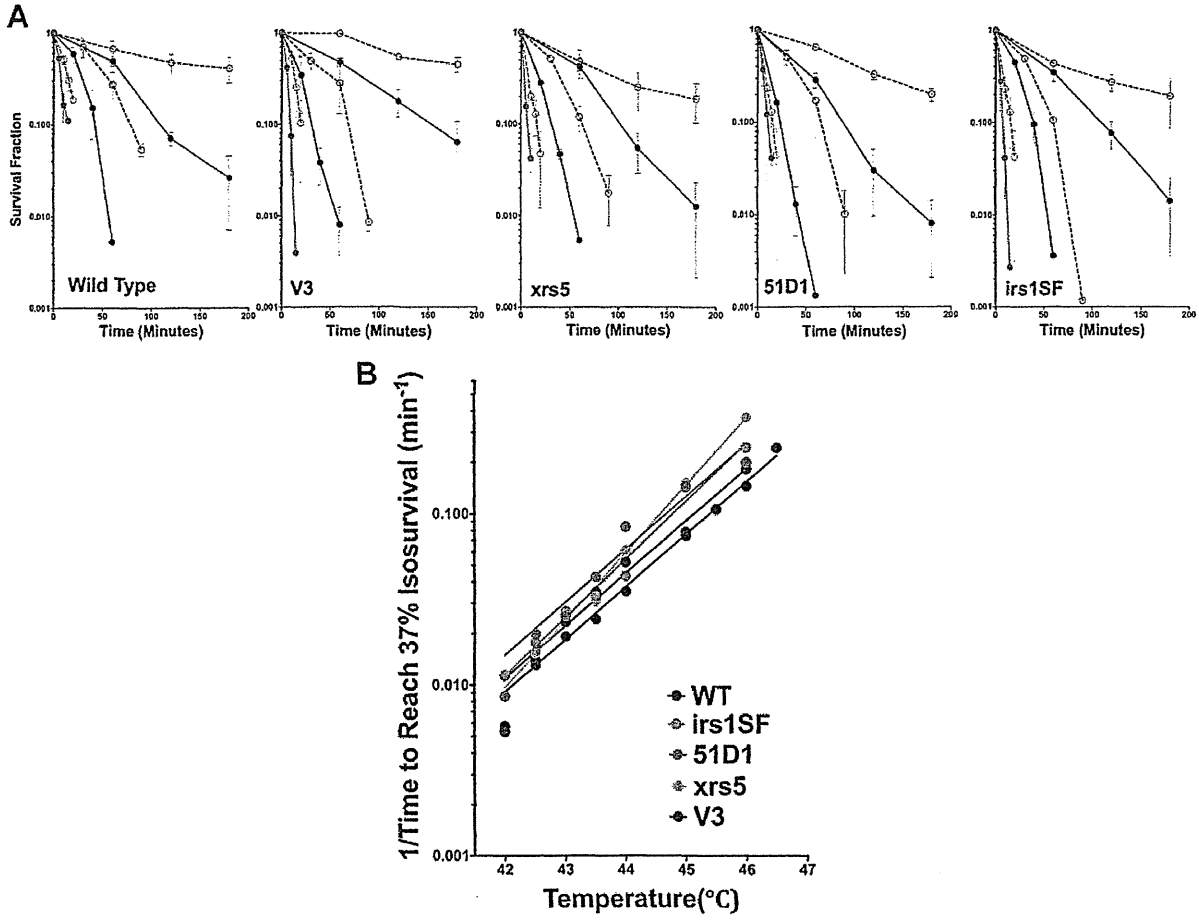

Fig. 1. A: Cell survival-heat only: Hyperthermia-induced cell killing was measured using a colony formation assay following exposure of cells to various times and temperatures of hyperthermic conditions. Graphical depictions are as follows: 42.0°C (open black circles, dotted black line), 42.5°C (closed black circle, solid black line), 43.0°C (open blue circles, dotted blue line), 44.0°C (closed blue circle, closed blue line), 45.0°C (open red circles, dotted red line), 46.0°C (closed red circles, closed red line). Note: Experiments were carried out at 0.5°C intervals from 42.0 to 46.5°C, but 1.0°C intervals were used to graphically represent data at and above 43.0°C for clarity. All experiments were carried out at least three times and error bars depict the standard error of the means. B: Inverse isosurvival plots-heat only: Inverse isosurvival plots were created from the results of the heat-only cell survival experiments for each cell line. Graphical depictions are as follows: A marked change was noted in data trends for wild-type cells, particularly data derived from 10% inverse iso-survival values, at and above temperatures of 42.0°C. All experiments were carried out at least three times.

intact. The presence of Rad51 in both the nucleus and cytoplasm of cells treated with 1 h of 42.5°C hyperthermia alone, or 1 h of 42.5°C hyperthermia following 1 Gy gamma-ray exposure and a 1 h 37°C incubation period was detected in both the nucleus and cytoplasm of treated wild-type cells after a given toxicological insult (assessed via Western blotting). This suggests that the immunocytochemistry data trend regarding Rad51's presence at double strand break sites in response to hyperthermia following radiation exposure is due to a loss-of-function dissociation of this protein from DNA double strand break sites.

Inverse isoeffect plots were created with 1/37% Rad51/γ-H2AX co-localizations (relative to background levels in un-heated 37°C irradiated cells) on the ordinate plotted against temperature on the abscissa (Fig. 4B). Rad51/γ-H2AX co-localization data were analyzed via an inverse isoeffect plot displaying a significant reduction of Rad51 DNA repair activity around 43°C, which in turn reflects a marked decrease in homologous recombination repair capabilities at and above this temperature. "1/time to reach isoeffect" values were represented as the inverse time of hyperthermia exposure required to reduce a population of cells' Rad51/γ-H2AX co-localization frequencies to 37% of wild-type CHO cells exposed to 1 Gy of gamma rays alone with no hyperthermic conditions (i.e., 37°C) following irradiation.

Exponentially proliferating wild-type cells were immediately exposed to varying hyperthermic conditions following exposure to 1 Gy of gamma rays. Unheated cells at 37°C showed a gradual diminishment of Rad51 activity over time post-irradiation. Cells heated at 42.5°C (40 or 60 min) and 44.5°C (20 or 40 min) displayed an initial loss and gradual restoration of Rad51/γ-H2AX co-localizations. At the 6-h time point, hyperthermic conditions of 42.5°C for 40 or 60 min had no significant differences with that of the control ($P > 0.05$), 44.5°C for 40 min resulted in significantly slower restoration of Rad51/γ-H2AX co-localizations than that of 42.5°C for 40 min ($P < 0.05$), 44.5°C for 20 min resulted in intermediate levels of co-localization restoration time and was significantly different from both 44.5°C for 40 min ($P < 0.01$) and 42.5°C for 40 min ($P < 0.001$). (*Note*: no post-irradiation 1-h incubation period

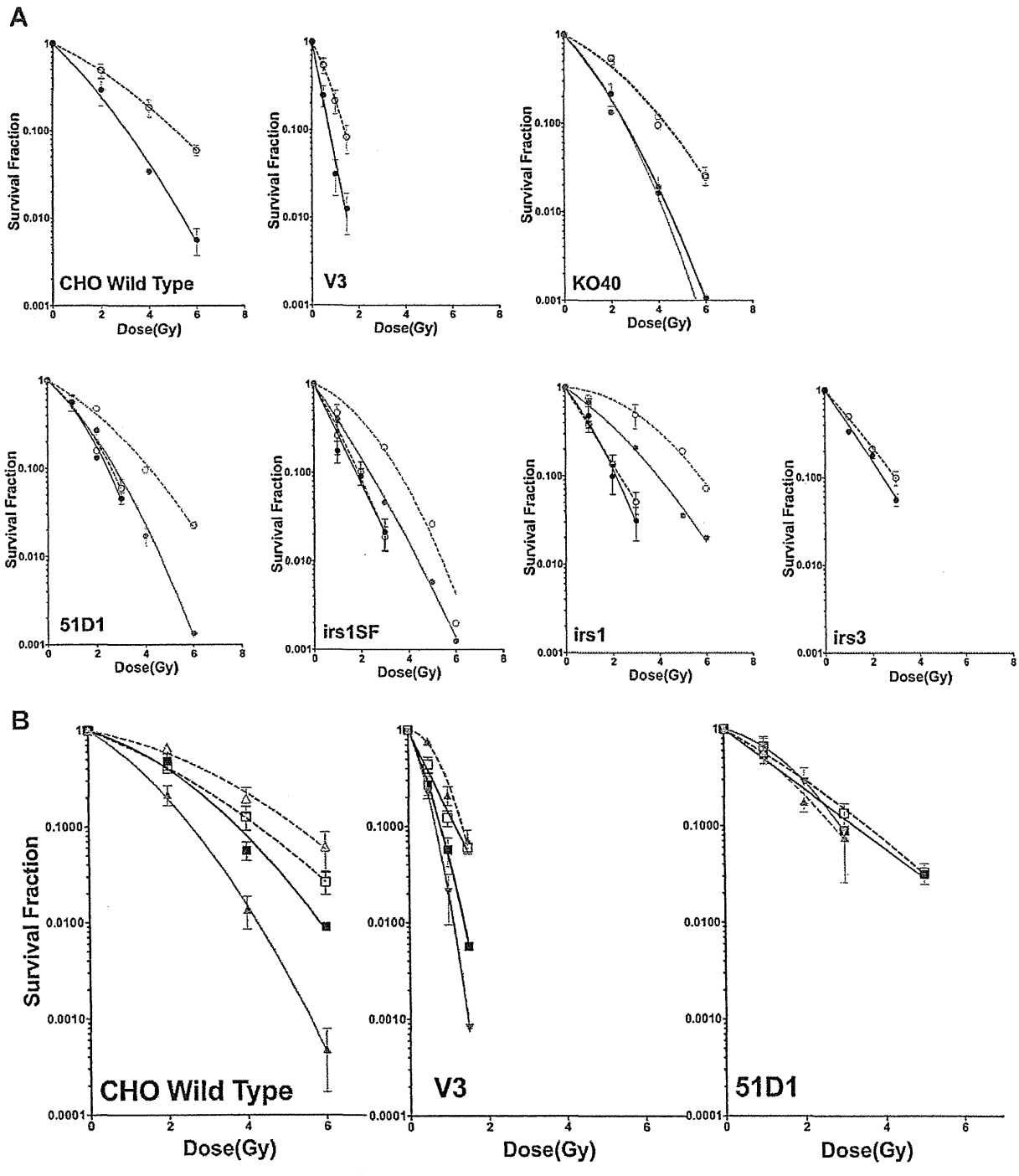

Fig. 2. A: Comparative cellular survival responses to radiation alone or radiation–hyperthermia conjunctive treatments in exponentially proliferating cell populations: Cells were exposed to 1 Gy of X-ray radiation alone or 1 Gy of X-ray radiation followed by exposure to 1 h 42.5°C hyperthermic conditions. Cell killing in response to various conditions was evaluated via a colony formation assay. Open circles/dotted lines represent samples exposed to radiation alone and closed circles/solid lines represent samples exposed to radiation and hyperthermia. Black lines represent mutant and wild-type samples and red lines represent gene-complimented samples. All experiments were carried out at least three times and error bars depict the standard error of the means. B: Evaluating hyperthermia-induced radio-sensitivities at various points in the cell cycle: synchronized cell populations in either G1 (black open squares/dotted line or black closed squares/solid line) or late S/G2 (red open circles/dotted line or red closed circles/solid line) were exposed to either 1 Gy of X-rays alone (all dotted lines) or 1 Gy of X-rays followed by exposure to 1 h of 42.5°C hyperthermic conditions (all solid lines). All experiments were carried out at least three times and error bars depict the standard error of the means.